Dalton Transactions

Hemilabile Bonding of 1-oxa-4,7-dithiacyclononane in Cyclometallated Palladium(II) Complexes

Journal:	*Dalton Transactions*
Manuscript ID	DT-ART-05-2019-002059.R1
Article Type:	Paper
Date Submitted by the Author:	01-Jul-2019
Complete List of Authors:	Janzen, Daron; St. Catherine University, Dept. of Chemistry and Biochemistry Bruening, Meaghan; St. Catherine University, Dept. of Chemistry and Biochemistry Mamiya, Arthur; Universidade Federal do Mato Grosso, Campus Ronodonopolis, Departamento de Matematica; Universidade de Brasília, Insitute of Physics Driscoll, Laura; St. Catherine University, Dept. of Chemistry and Biochemistry DA SILVA FILHO, DEMETRIO; Universidade de Brasília, Institute of Physics; University of Brasilia, International Center for Condensed Matter Physics

Hemilabile Bonding of 1-oxa-4,7-dithiacyclononane in Cyclometallated Palladium(II) Complexes

Daron E. Janzen[a*], Meaghan A. Bruening[a], Arthur A. Mamiya[b,c], Laura E. Driscoll[a], Demetrio A. da Silva Filho[c,d]

[a] **Department of Chemistry and Biochemistry, St. Catherine University, St. Paul, MN, USA**

[b] **Departamento de Matemática, Universidade Federal do Mato Grosso - Campus Rondonópolis, Rondonópolis, Brazil**

[c] **Institute of Physics, University of Brasilia, 70910-900, Brasilia, Brazil**

[d] **International Center for Condensed Matter Physics, Universidade de Brasilia, CP 04455, 70919-970 - Brasilia, Brazil**

*** Corresponding author Address: Department of Chemistry and Biochemistry, St. Catherine University, St. Paul, MN 55105, USA. Tel.: +1 651 690 6047; fax: +1 651 690 8657. E-mail address: dejanzen@stkate.edu**

Keywords: 1-oxa-4,7-dithiacyclononane, 1,4,7-trithiacyclononane, palladium complexes, cyclometallating ligands, X-ray crystal structures, DFT calculations

Abstract

The synthesis and characterization of a series of cyclometallated complexes of Pd(II) incorporating the mixed donor ligand 1-oxa-4,7-dithiacyclononane ([9]aneS_2O) are presented in this study. Complexes of the form [Pd(C^N)([9]aneS_2O]((PF_6) (C^N = 2-phenylpyridine (ppy) **1b**, 4-(2-pyridyl)benzaldehyde (ppyCHO) **2b**, 7,8-benzoquinoline (bzq) **3b**, 2-benzothienylpyridine (btp) **4b**, 2-phenylbenzothiazole (pbt) **5b**), were obtained in high-yield from a simple two-step synthetic scheme. All of these complexes were fully characterized by NMR, ESI-MS, IR, combustion analyses, and most (**1b**, **2b**, **4b**, **5b**) by X-ray crystallography. Solution ^{1}H and ^{13}C NMR of [Pd(C^N)([9]aneS_2O]((PF_6) complexes demonstrate complicated [9]aneS_2O behavior at room temperature. Variable temperature NMR reveals dynamic bonding of the [9]aneS_2O ligand consistent with the presence of both *endodentate* and *exodentate* bonding modes. This is in stark contrast to the related [9]aneS_3 (1,4,7-trithiacyclononane) cogeners that demonstrate fluxional *endodentate* bonding only in solution. X-ray structures reveal only *exodenate* [9]aneS_2O bonding in this series, unlike the related [9]aneS_3 complexes that show *endodenate* bonding with an axial Pd…S interaction. DFT calculations performed on *endo* and *exo* [9]aneS_2O bonding forms of **4b**, as well as a transition state calculation for interconversion, suggest reasonable access to both bonding forms based on the energy barrier. Natural Bond Order calculations provide further evidence for a weak axial Pd…O interaction in the *endo* form of **4b**.

Introduction

Palladium catalysts used for a variety of organic transformations including C-H bond activation[1,2] and oxidative cross-coupling reactions[3] rely on the $Pd^{II/IV}$ redox couple and the coordination preferences of each oxidation state. More recently, cyclometallated palladium systems have shown evidence suggesting the Pd(III) oxidation state can play an important role in catalysis.[4,5,6,7] Our previous studies of cyclometallated Pd(II) complexes with [9]aneS_3 (1,4,7-trithiacyclononane) have shown unusual well-defined sequential 1-e- reversible $Pd^{II/III}$ and $Pd^{III/IV}$ electrochemistry, suggesting some stability of a potentially five-coordinate Pd(III) species[8,9] Solid-state structural evidence also suggests axial Pd...S interactions of [9]aneS_3 play a key role in this behavior. The vast majority of structures of d^8 metal complexes with [9]aneS_3 demonstrate that the ligand forms two M-S bonds with a third M…S interaction longer than a bond but significantly shorter than the sum of van der Waals radii. The disparity between the electronic preferences of square planar d^8 ions and the *endodentate* geometric preference of the [9]aneS_3 ligand permits stabilization of related complexes in unusual oxidation states such as Pd(III),[10] Pt(III),[11] and Au(II).[12]

While the coordination chemistry of [9]aneS_3 has been studied widely, reports of metal complexes of related mixed donor tridentate macrocyclic ligands such as [9]aneS_2N ([9]aneS_2N = 1-aza-4,7-dithiacyclonone)[13] and [9]aneS_2O ([9]aneS_2O = 1-oxa-4,7-dithiacyclononane) are sparse. Several bis-homoleptic complexes of [9]aneS_2O with first-row transition metals are reported (Co(II),[14] Ni(II),[15] Cu(I),[14] Cu(II)[15)] as well as 4d and 5d metals (Hg(II),[16] Cd(II),[16] Au(I),[17] Au(II),[17] Au(III),[17] Pt(II),[18] and Pd(II)[18]). Very few heteroleptic metal complexes of [9]aneS_2O are reported. Unlike complexes of [9]aneS_3 which almost exclusively display *endodentate* ligand conformations, [9]aneS_2O can bind in both *exodentate* and *endodentate*

fashion. While the *endo*/*exo* preference of bonding [9]aneS_2O to transition metals likely involves the coordination number and stereochemical preferences of the metal and hard/soft compatibility, d^8 metal complexes present additional complexity with the possibility of axial interactions. Of particular interest are the complexes Pt([9]aneS_2O)Cl_2 and Pd([9]aneS_2O)Cl_2.[19] Both of these complexes have been crystallographically characterized in a form with *endodentate* [9]aneS_2O coordination and another form with an *exodentate* [9]aneS_2O ligand conformation. As minimally higher crystal growth temperatures favored the *exodentate* conformations in each complex (lacking an axial M…O interaction), the presence of oxygen atom interactions with the d^8 metal center for the thermodynamically more stable *endodentate* conformation suggests a subtle interplay between preferred ligand conformation and the strength of the M…O interaction. Heteroditopic ligands, including [9]aneS_2O, can be considered hemilabile and this behavior could be exploited in complexes for catalysis.[20,21]

As Pd(III) is expected to prefer hard Lewis base donor atoms compared with Pd(II), we postulated that a mixed donor macrocycle of the same size that includes softer sulfur donors and a harder oxygen donor might provide enhanced stability for a potentially stabilized Pd^{III} species. In an effort to probe these potential axial donor effects, we studied a series of heteroleptic palladium complexes of the form [Pd(C^N)([9]aneS_2O)](PF_6) (C^N = cyclometalating ligand with carbonanion and nitrogen donors) with a variety of C^N ligands including 2-phenylpyridine (ppy), 7,8-benzoquinoline (bzq), 2-benzothienylpyridine (btp), 2-phenylbenzothiazole (pbt), and 4-(2-pyridyl)benzaldehyde (ppyCHO) (Scheme 1).

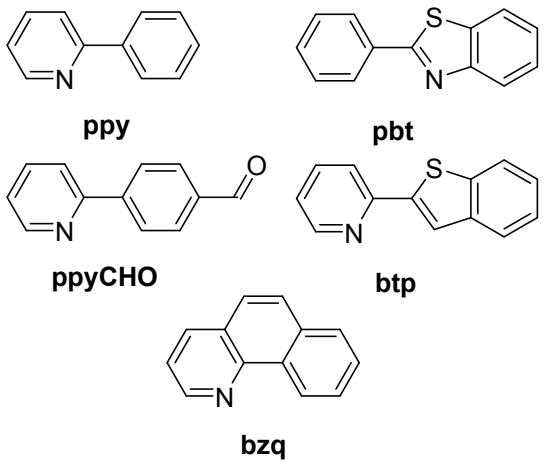

Scheme 1

Some of these potentially cyclometallating ligands were chosen so comparisons could be made between [9]aneS_2O and previously studied [9]aneS_3 palladium complexes.[8,9] Also, all these cyclometallating ligands are planar, preventing the introduction of further steric effects, and are all commercially available. While cyclometallation chemistry of most of these ligands is common, Pd(II) chemistry with thienylpyridine[22,23,24] ligands is relatively rare. Study of cyclometallated ppyCHO is unknown at Pd(II), but limited examples of Pt(II),[25] Ir(III),[26] and Ru(II)[27] complexes are reported.

Results and Discussion

Syntheses

The synthesis of cyclometallated palladium(II) complexes with [9]aneS_2O proceeds by a two-step method we have developed previously[8] for analogous [9]aneS_3 complexes, shown in Scheme 2.

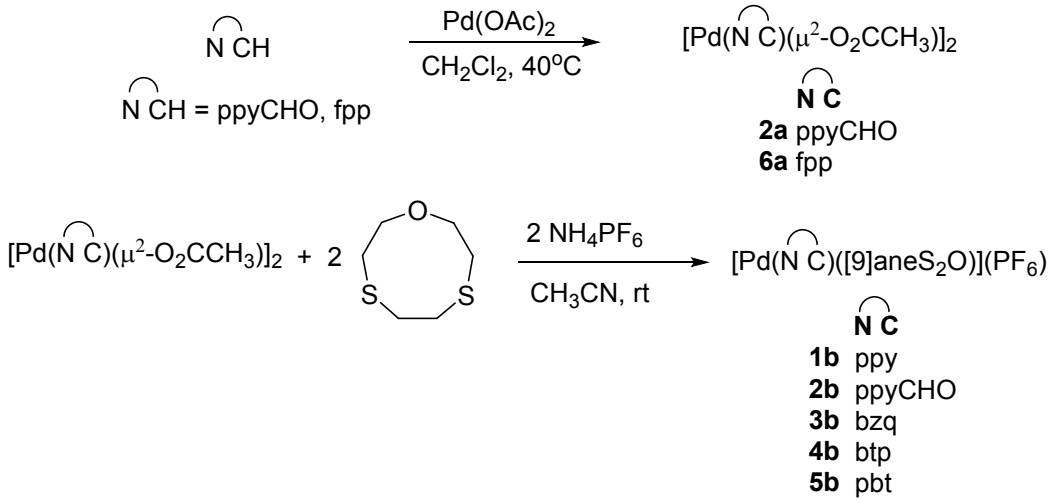

Scheme 2

The mild low-temperature route for C-H activation of the neutral protonated form of the potentially cyclometallating ligand with palladium(II) acetate in CH_2Cl_2 proceeds cleanly in high yields to form binuclear bis-μ-acetato-bridged complexes. We previously reported the preparation of the complexes $[Pd(C^N)(\mu\text{-}O_2CCH_3)]_2$ (where C^N = ppy, bzq, btp, and pbt).[8] This study extends this synthetic scheme to include the preparation of $[Pd(C^N)(\mu\text{-}O_2CCH_3)]_2$ (where C^N = ppyCHO (**2a**), fpp (**6a**); ppyCHO = 4-(2-pyridyl)benzaldehyde; fpp = 2-[4-(trifluoromethyl)phenyl]pyridine). It is clear that this synthetic method is tolerant of both moderate and strongly electron-withdrawing functional groups as demonstrated with the aldehyde group of ppyCHO and the trifluoromethyl group of fpp. A combination of combustion analyses, X-ray crystal structures, and NMR characterization confirmed the dimeric composition of complexes **2a** and **6a**. To our knowledge, **6a** is the first report of a cyclometallated fpp complex of Pd(II).

Ligand substitution reactions of appropriate acetate bridged dimers (or $[Pd(ppy)Cl]_2$ for ppy ligand) with $[9]aneS_2O$ in a 1:2 molar ratio at room temperature in CH_3CN followed by

anion metathesis using hexafluorophosphate affords the complexes [Pd(C^N)([9]aneS_2O)] (PF_6) (C^N = ppy (**1b**), ppyCHO (**2b**), bzq (**3b**), btp (**4b**), pbt (**5b**)) for all cyclometallating ligands of this study *except* fpp. The complexes **1b-5b** were all obtained in high yields. No product of the form [Pd(fpp)([9]aneS_2O)](PF_6) was either isolated or detected spectroscopically (NMR, ESI-MS) in solution. Further attempts to produce [Pd(fpp)([9]aneS_2O)](PF_6) including longer reaction times and heat were also not successful. The same problems were encountered in attempts to synthesize the [9]aneS_3 analog using **6a**, resulting in no evidence of the formation of [Pd(fpp)([9]aneS_3)](PF_6). While crude products **1b**-**5b** were obtained in high purity, further purification was achieved by recrystallization using nitromethane/diethyl ether or slow evaporation from acetonitrile. For comparison with the [9]aneS_2O complex **2b**, the complex [Pd(ppyCHO)([9]aneS_3)](PF_6) **2c** was prepared using the same procedure except for using the solvent CH_3NO_2. Complexes **1b**-**5b** and **2c** were fully characterized by combustion analyses, ATR-IR, and ESI-MS. The identity of the molecular monocation of each complex was confirmed by observation of the expected mass and isotopic pattern based on the predicted formulas.

NMR Spectroscopy

[Pd(C^N)(μ-O_2CCH_3)]$_2$ Complexes

Proton and carbon NMR spectroscopy confirmed cyclometallation and assembly of the [Pd(C^N)(μ-O_2CCH_3)]$_2$ complexes **2a** and **6a**. Figures S1 and S2 show the ^{1}H NMR spectra of **2a** and **6a**, respectively. The cyclometallation is confirmed as each aromatic ligand displays one less ^{1}H resonance than the corresponding free ligand and downfield coordination induced chemical shifts are typical to those previously observed.[8] Two sets of aromatic peaks are present, as expected for *syn* and *anti* isomers of these dimers (Scheme S1). The major isomer

present in solution is the *anti* isomer, as confirmed by the larger integration of the two equivalent acetate methyl groups compared with the sum of the integration of the inequivalent acetate methyl groups of the *syn* isomer. Based on the acetate resonances, the *anti*/*syn* ratio is about 5:1 for **2a** and 10:1 for **6a**. Carbon NMR of **2a** and **6a** (Figures S3 & S4, respectively) and fluorine NMR of **6a** (Figure S5) are consistent with the presence of two isomers with a predominance of the *anti* isomer. The lower symmetry of the bridging acetate groups of the *syn* isomer is seen in both the carboxylate and methyl carbons of the ^{13}C spectrum. The low solubility of **6a** in CD_2Cl_2 precluded acquisition of a high-quality ^{13}C spectrum.

[Pd(C^N)([9]aneS$_2$O)](PF$_6$) Complexes

Room temperature ^1H NMR of the complexes [Pd(C^N)([9]aneS$_2$O)](PF$_6$) clearly demonstrates the bonded cyclometallating ligand is retained with small but significant changes in the aromatic region associated with ligand exchange of acetate for [9]aneS$_2$O. Proton resonances in the region of the coordinated [9]aneS$_2$O ligand are shifted relative to the free ligand (3.88 ppm (-C*H*$_2$OC*H*$_2$-), 3.02 ppm (-SC*H*$_2$C*H*$_2$S-), 2.77 ppm (-OCH$_2$C*H*$_2$S-) in CD_3NO_2) but show complicated behavior. Figure 1 shows the ^1H NMR spectrum of **2b** as a typical example. The spectrum shows seven inequivalent aromatic protons of the coordinated ppyCHO ligand with integration, chemical shifts, peak widths, and spin-spin splitting as expected. The singlet at 7.91 ppm partially overlaps with a doublet at 7.94 ppm. The aldehyde proton appears as a single peak with a chemical shift further downfield (9.93 ppm). Comparison with the aliphatic region indicates complicated behavior of the coordinated [9]aneS$_2$O, with the presence of peaks with large variable widths. A simple interpretation of the narrowest peaks in this region (4.45, 4.00, 3.38 ppm) might suggest these represent an *exodentate* conformation of the coordinated [9]aneS$_2$O.(Scheme 3)

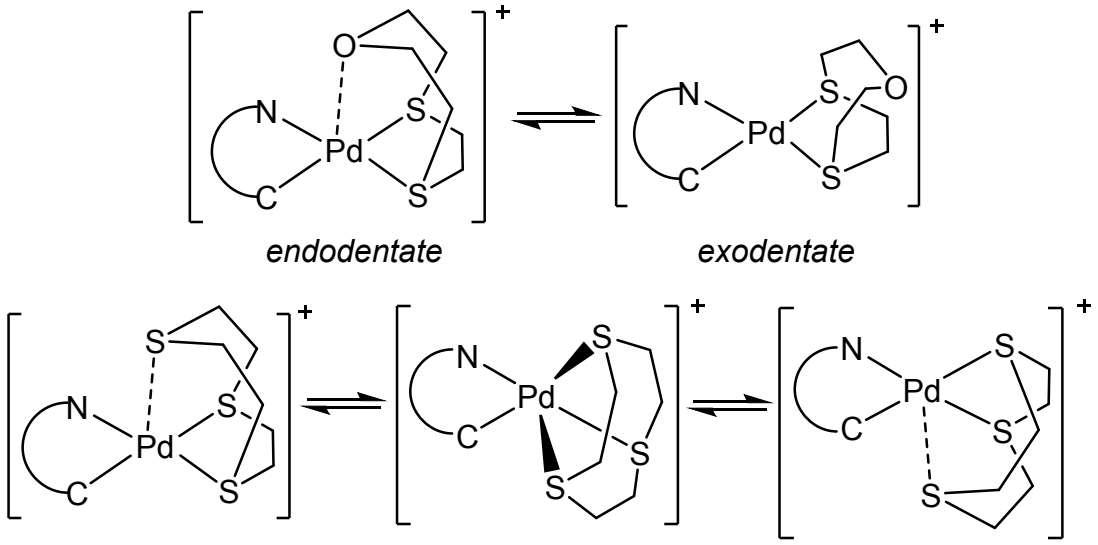

Scheme 3: Endodenate/Exodentate Equilibrium Behavior of [9]aneS_2O Contrasted with Fluxional Behavior of [9]aneS_3 in Palladium(II) Cyclometallated Complexes

The resonance at 4.45 ppm is assigned as the four hydrogens of carbons 2 and 9 of the macrocycle and is shifted downfield compared to the analogous peak of the free ligand (3.88 ppm). The resonance at 4.00 ppm is assigned as the four hydrogens of carbons 3 and 8 of the macrocycle ligand and is shifted considerably downfield compared to the free ligand (2.77 ppm). The resonance at 3.38 ppm is assigned as the four hydrogens of carbons 5 and 6 of the macrocycle is shifted least downfield of the coordinated [9]aneS_2O ligand compared to the resonance of the free ligand (3.02 ppm). *Exodentate* coordination of [9]aneS_2O in **2b** contrasts with the previous report of Pd([9]aneS_2O)$Cl_2$14 where the solution macrocycle conformation was assigned as *endodentate*, consistent with the only X-ray structure known at the time of publication. A simple analysis of the spin-spin splitting patterns of these peaks in **2b** are also not consistent with this assignment. However, metal complexes of mixed donor macrocycles such as [9]aneS_2O have been shown to exhibit one of several ligand conformation possibilities in X-ray structural data.[28] Allowing for dynamic ligand conformers as well as observation of large peak

widths suggest dynamics are present in the ethylene straps of the coordinated [9]aneS_2O. Selective proton decoupling experiments confirmed coupling of the resonances at 4.45 ppm and 4.00 ppm and no coupling of either of these with the resonance at 3.38 ppm. This interpretation does not account for the extremely broad signal in the 3.45-3.95 ppm region or the broad resonance at 3.27 ppm. Integration of the three assigned resonances of an *exodentate* form of [9]aneS_2O in **2b** account for 50% of the population of the sample (6H of 12H) based on comparison with the aromatic region (each nonequivalent aromatic resonance as one proton). If the broad regions integrations are summed, they account for the remaining 6 protons for the expected btp:[9]aneS_2O stoichiometry of the compound.

Carbon NMR at room temperature (Figure 2) showed analogous behavior with the presence of the expected number of peaks in the aromatic region (11 inequivalent resonances) and an aldehyde carbon peak at 194.04 ppm. The aliphatic [9]aneS_2O portion of the spectrum shows six broad peaks shifted downfield relative to the free ligand (74.93 ppm, 35.81 ppm, 34.26 ppm). To be consistent with the ^{1}H NMR interpretation of *exodentate* [9]aneS_2O , the two broad resonances near 77 ppm, and four broad resonances between 36-46 ppm would be assigned as the carbons in the 2 and nine positions, and 3,5,6,8 positions, respectively. The large peak widths again indicate the possibility of dynamics in the bound [9]aneS_2O ligand. The six broad carbon peaks could be consistent with one of two possible explanations. The presence of six peaks could be the result of a single solution species bearing a coordinated [9]aneS_2O ligand with the lack of axial symmetry enforced by the cyclometallating ppyCHO ligand or the presence of two nonidentical similar dynamic species in similar population, each with 3 unique ^{13}C environments for the [9]aneS_2O ligand. The second explanation could account for the presence of both *endo* and *exo* conformers.

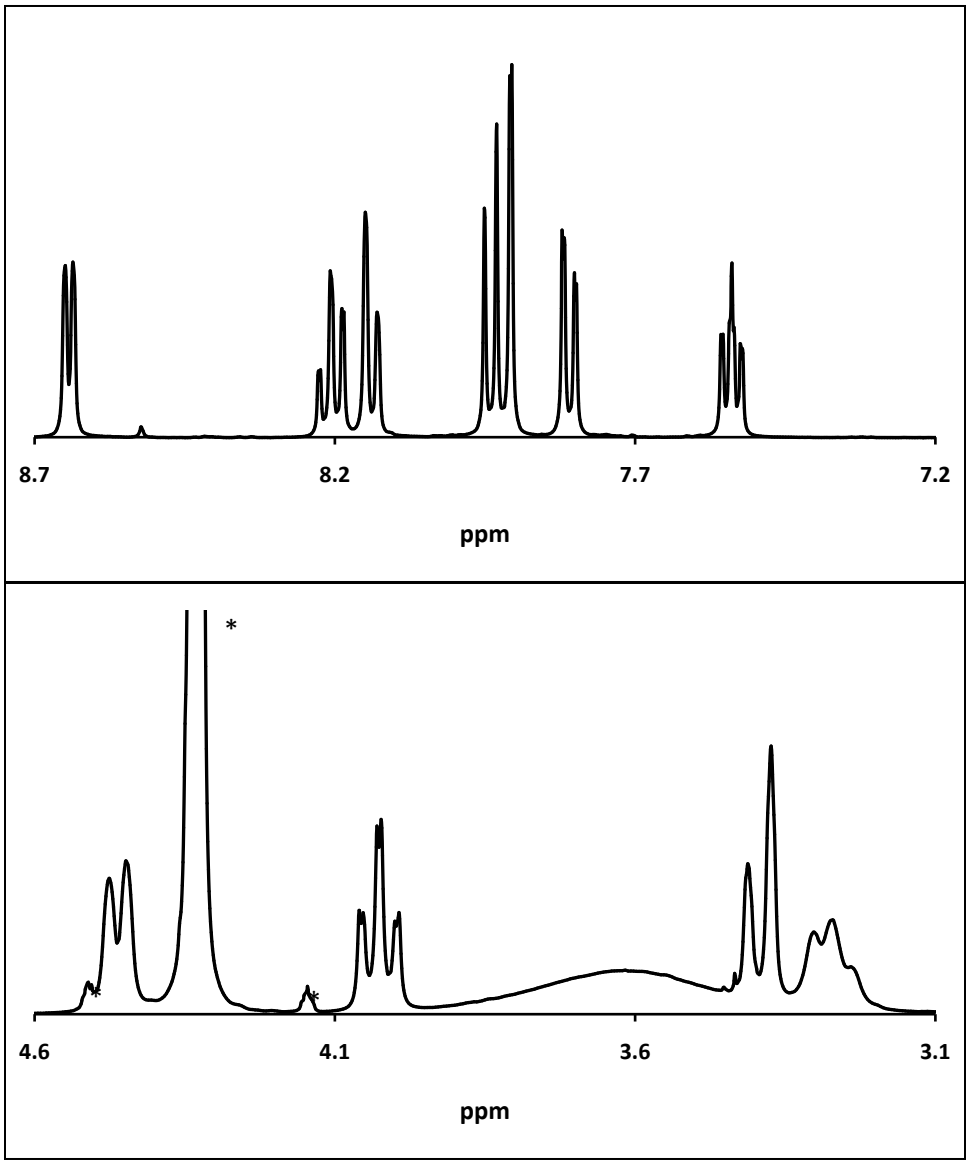

Figure 1. ^{1}H NMR of [Pd(ppyCHO)([9]aneS_2O](PF_6) (2b), in CD_3NO_2 at 23^{o}C. *Top*: aromatic region. *Bottom*: Coordinated [9]aneS_2O region. Both plots retain the same ppm and intensity scales. * indicates peaks associated with residual CD_2HNO_2.

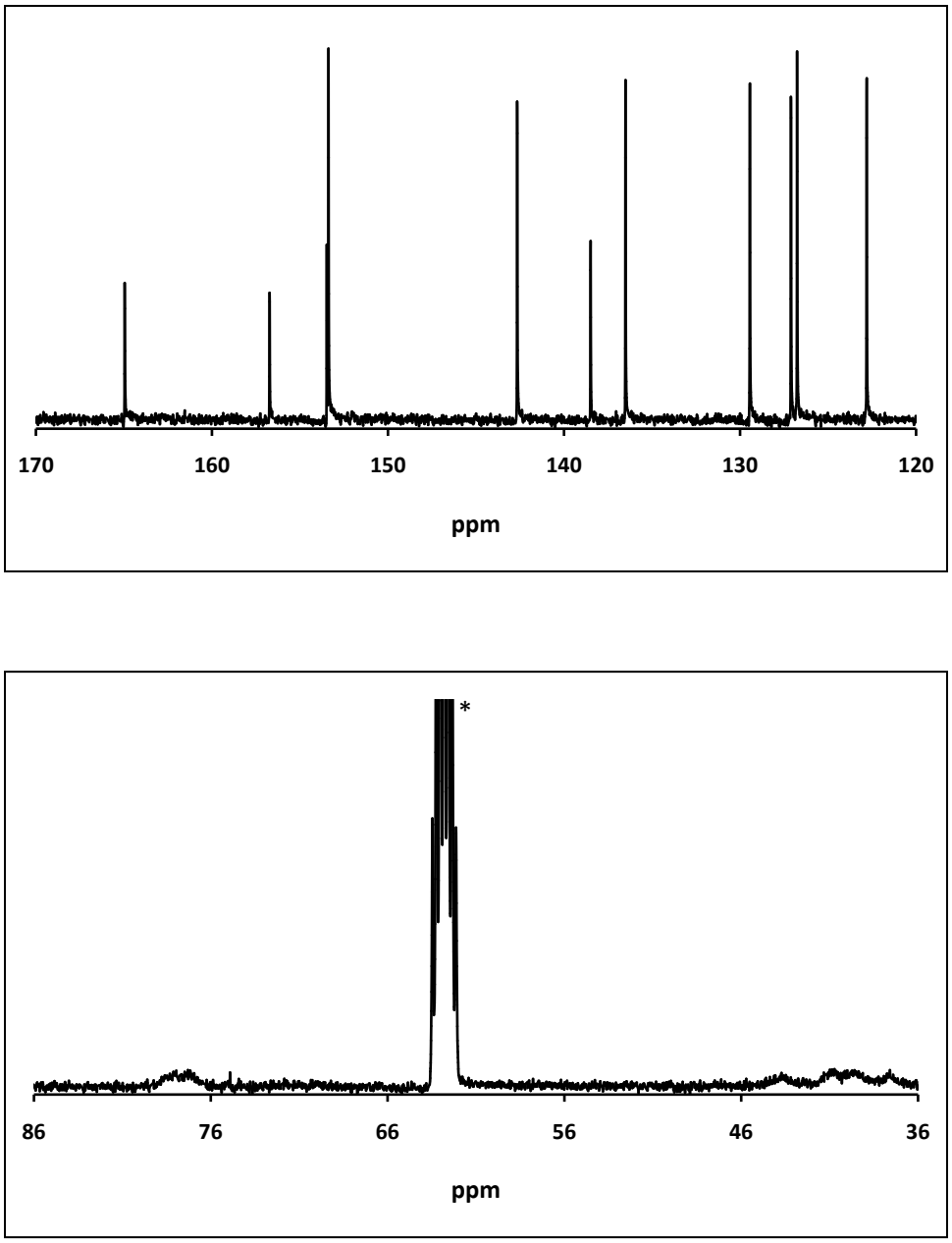

Figure 2. ^{13}C NMR of [Pd(ppyCHO)([9]aneS_2O](PF_6) (2b), in CD_3NO_2 at 23°C. *Top*: aromatic region. Two nearly overlapping peaks near 154 ppm. *Bottom*: Coordinated [9]aneS_2O region. Both plots retain the same ppm and intensity scales. * indicates peaks associated with residual CD_2HNO_2.

Variable Temperature NMR of [Pd(C^N)([9]aneS$_2$O)](PF$_6$) Complexes

To further investigate the dynamic behavior of the [9]aneS$_2$O ligand, we performed a variable temperature ^{1}H NMR study. Figure 3 displays the aliphatic region of the ^{1}H NMR of complex **2b** in CD_3NO_2 in a range from -15°C to 70°C.

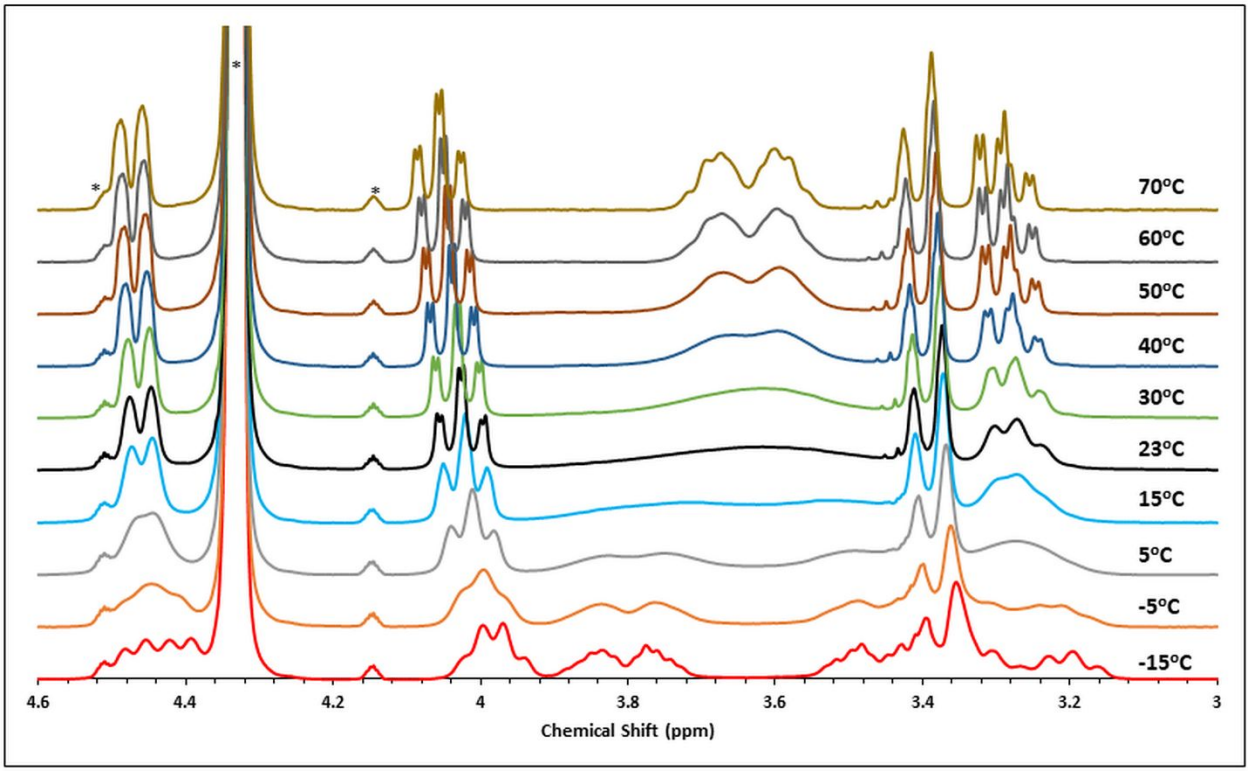

Figure 3. Variable temperature ^{1}H NMR of [Pd(ppyCHO)([9]aneS$_2$O](PF$_6$) (2b), in CD_3NO_2, aliphatic region. * indicates peaks associated with residual CD_2HNO_2.

Small chemical shift changes are observed for all aromatic proton resonances, but the number of peaks, integrations, and splitting remain the same across all temperatures, with some reasonable broadening at higher temperatures. The aliphatic region, however, shows large changes in this temperature range. Assuming the interpretation that peaks near 4.45, 4.00, and 3.40 represent an *exodentate* form of the bonded [9]aneS$_2$O ligand, these resonances appear to show small monotonic chemical shift changes with temperature, broaden at temperatures below

23°C, then demonstrate more complexity with inequivalence present in a more rigid *exodentate* metal complex at -15°C. The remaining peaks at 70°C, in the region near 3.64 ppm and 3.25 ppm, are assigned as an *endodentate* conformation of the bound ligand [9]aneS_2O. These peaks account for the integration of 4 and 2 hydrogens, respectively. The complex symmetric peak centered at 3.64ppm (70°C) broadens, coalesces near 23°C, then splits into two resonances at 3.80 ppm and 3.48 ppm. The peak at 3.25 ppm (70°C) coalesces near the same temperature, splitting into a complicated feature near 3.19 and 3.32 ppm. This temperature dependent behavior of the *endodentate* conformation is interpreted as fast fluxional behavior of the *endodenate* [9]aneS_2O at higher temperatures, coalescence at temperatures near room temperature as the barrier to 1,4-metallotropic shifts is approached, and a nonfluxional *endodentate* conformation is observed at the lowest temperatures.

The dynamic behavior of *endodentate* [9]aneS_2O has not been observed previously. Only two other relevant examples of palladium [9]aneS_2O complexes exist. The NMR of the homoleptic bis complex [Pd([9]ane$S_2O)_2$]$(PF_6)_2$18 is reported as consistent with the *exodentate* X-ray structure, though the authors also note that ^{1}H NMR cannot differentiate between *exodentate* and *endodentate* coordination modes. This may be true for bis homoleptic complexes of [9]aneS_2O but not in general. The complex Pd([9]aneS_2O)Cl_2, of which polymorphs of *endodentate* and *exodentate* forms are now known,19 is reported as consistent with the *endodentate* [9]aneS_2O geometry of the only known structure at that time.[14] As the growth of *endodentate* and *exodentate* Pd([9]aneS_2O)Cl_2 polymorphs is controlled by small changes in crystal growth temperature (higher temperature favors *exodentate* form), simultaneous thermodynamic access to both bound ligand conformations is possible. If the barrier in fact to interconversion between *exo*-**2b** and *endo*-**2b** is sufficiently low, at equilibrium, the population

of the two conformers should change as a function of temperature, assuming one conformer is more stable than the other as expected. Based on integration of the ^{1}H NMR, the population of the *endo* and *exo* forms of **2b** are essentially unchanged and nearly equal across the temperature range. To explain this apparent temperature insensitivity to equilibrium population in this temperature range, both $\Delta H^{\ddagger}$ and $\Delta S^{\ddagger}$ are required to be small. Subtle intramolecular geometry differences between the *endo* and *exo* forms and flexibility of the nine-membered macrocycle ring could justify a small $\Delta S^{\ddagger}$. A small $\Delta H^{\ddagger}$ for *endo/exo* conversion is also reasonable as the enthalpy required to overcome the expected weak axial Pd…O interaction present in the *endo* form to reach the *exo* form should be minimal.

A barrier for the dynamic fluxional behavior of *endodentate* **2b** can be estimated from the coalescence temperatures of the *endo* [9]aneS_2O NMR resonances according to the equation $\Delta G^{\ddagger} = RT_c[22.96+\ln(T_c/\delta\nu)]$ in J/mol.[29] The free energy of activation calculated from the NMR at the coalescence temperatures suggests a barrier of approximately 12 kcal/mol. A lower barrier of approximately 9 kcal/mol has been estimated for the fluxional *endodentate* behavior of [9]aneS_3 in the complex [Pt(phen)([9]aneS_3)]$(PF_6)_2$ with an even lower barrier for [Pd(bpy)([9]aneS_3)]$(PF_6)_2$.[30]

Further NMR studies were performed to determine if the NMR behavior of **2b** is similar to others in this series of [9]aneS_2O complexes. Variable temperature ^{1}H NMR spectra were acquired for the complex [Pd(pbt)([9]aneS_2O)](PF_6) (**5b**) in the range of 5°C to 50°C (Fig S6). Similar behavior is observed, consistent with the interpretation of the VT-NMR of **2b**. As several peaks of [9]aneS_2O overlap with solvent of crystallization and NMR solvent, and peaks attributed to *endo* and *exo* forms overlap, further analysis including integration of peaks to

determine populations of the two forms is precluded. Variable temperature proton NMR spectra of **3b** were recorded in the range of 22°C to 75°C (Fig. S7). While the 22°C spectrum **3b** is difficult to interpret with overlapping broad [9]aneS_2O peaks, the high-temperature spectrum of **3b** is quite similar to that of **2b**. In a series of variable temperature ^{1}H NMR spectra collected of **4b** (0°C to 50°C, Fig. S8) all peaks of the [9]aneS_2O region are very broad near room temperature. This behavior is in contrast with complexes **2b**, **3b**, and **5b**. Interesting changes are also observed in the [9]aneS_2O region of the ^{13}C NMR of **4b** with changes in temperature (Fig. S9). The carbon NMR of **4b** shows a progression from a six peak spectrum of broad line widths at 0°C, to broader peaks at 22°C, and finally to the absence of [9]aneS_2O peaks at 50°C. At least small differences in fluxional *endodenate* [9]aneS_2O and/or *endodentate/exodentate* equilibria are expected as a function of the cyclometallated ligand. In the case of **4b**, the temperature dependent ^{1}H and ^{13}C NMR are consistent with similar barriers for both types of processes.

[Pd(ppyCHO)([9]aneS_3)](PF_6)

The NMR of cyclometallated [9]aneS_3 complexes of Pd(II) and Pt(II) have been reported by our group previously.[8,9] As a means for direct comparison with the complex [Pd(ppyCHO)([9]aneS_2O](PF_6) **2b**, we synthesized the [9]aneS_3 analog [Pd(ppyCHO)([9]aneS_3](PF_6) **2c** and present the ^{1}H and ^{13}C NMR in Figure S10. The ^{1}H NMR of **2c** in the aliphatic region shows a highly symmetric AA'BB' peak pattern consistent with a fluxional *endodentate* [9]aneS_3 ligand. No evidence of an *exodentate* form is present. The ^{13}C NMR of **2c** displays a single peak for the six equivalent methylene carbons of the fluxional

endodentate [9]aneS$_3$ ligand. Assignment of the *endodentate* conformation of [9]aneS$_3$ is consistent with the X-ray structure of **2c** as well. All other reported complexes of Pt and Pd with [9]aneS$_3$ and cyclometallated ligands and related diimine ligands[30,31,32,33,34,35,36] show the same solution behavior in ^{1}H and ^{13}C NMR. We have noted that the lack of axial mirror symmetry in this cyclometallated complex (and previously reported complexes) is not manifested in lower symmetry of the fluxional [9]aneS$_3$ as the ^{13}C NMR spectrum indicates only a single averaged ^{13}C environment. Lack of any solution NMR evidence of *exodentate* [9]aneS$_3$ compared with [9]aneS$_2$O suggests that axial Pd…S interactions may be stronger than analogous axial Pd…O interactions.

X-ray Structures

A summary of data collection and refinement for five X-ray structures collected on complexes of the form [Pd(C^N)([9]aneS$_2$O)](PF$_6$) (**1b**, **2b**, **4b*CH$_3$CN, 4b*CH$_3$NO$_2$, 5b*CH$_3$NO$_2$**) are presented in Table 1. Table S1 includes data collection and refinement for X-ray structures of the acetate bridged-dimers **2a** and **6a**, as well as the [9]aneS$_3$ complex **2c**.

[Pd(C^N)(μ-O$_2$CCH$_3$)]$_2$ complexes

The structures of [Pd(ppyCHO)(μ-O$_2$CCH$_3$)]$_2$ (**2a**) and [Pd(fpp)(μ-O$_2$CCH$_3$)]$_2$ (**6a**) were collected as synthetic intermediates in the preparation of subsequent [9]aneS$_2$O complexes. An anisotropic thermal displacement ellipsoid diagrams of **2a** is shown in Figure 4 (**6a** in Figure S11).

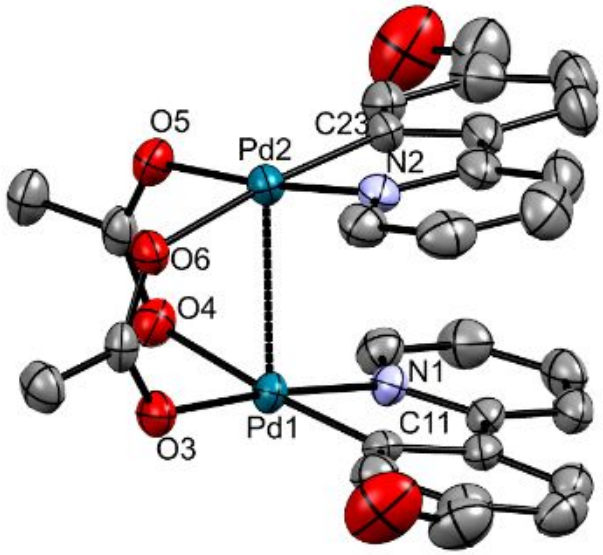

Figure 4. Thermal ellipsoid perspective of [Pd(ppyCHO)(μ-O_2CCH_3)]$_2$ (2a) (50% probability, H atoms omitted for clarity).

These dimer structures consist of two four-coordinate approximately square pyramidal Pd(II) centers, each with a chelating cyclometallating ligand, two bridging acetate groups, and a short axial Pd…Pd interaction. The *anti* isomer is observed exclusively in each structure, where the cyclometallating ligands of a dimer are related by a non-crystallographic 2-fold axis. The *anti* isomer is commonly observed for these types of cyclometallated dimers. In the case of **2a** and **6a**, these structures additionally have steric constraints arising from the substituents in the 4-position of the phenyl ring of the cyclometallating ligands, consistent with the observed *anti* isomer in the solid-state. In the structure of **6a**, the aldehyde groups are nearly planar with the phenylpyridine ligands (torsion angles C22-C21-C24-O2 = -1.9(9)°, C10-C9-C12-O1= 5.3(8)°) and carbonyl groups are directed toward the Pd in the coordination plane. Typical Pd-N and Pd-C bond lengths are observed for μ-acetate bridged complexes of this type. The pattern of longer

Pd-N bonds and shorter Pd-C bonds is reasonable given the carbanionic character of the Pd bonded carbon atoms of these ligands. The Pd-C bonds of **6a** (Pd1-C11 = 1.959(7) Å, Pd2-C23 = 1.948(5) Å) are quite similar to those of **2a** (Pd1-C11 = 1.955(4) Å, Pd2-C23 = 1.970(4) Å). These Pd-C bond lengths are also analogous to other cyclometallated Pd complexes, suggesting minimal effects on the Pd-C bonds of the strong electron-withdrawing CF_3 and moderately electron-withdrawing aldehyde groups. Likewise, the Pd-O bonds *trans* to the stronger σ-donor Pd-C bonds are slightly longer (≈ 0.1 Å) than the Pd-O bonds *trans* to the Pd-N bonds. As these dimers adopt a sandwich-type structure, short intramolecular Pd…Pd contacts are present. The Pd…Pd separations (**6a** = 2.8673(7) Å, **2a** = 2.8553(5) Å) are shorter than the van der Waals radii sum for two Pd atoms (3.26 Å). The angle between least-squares planes of the cyclometalating ligands (**6a** = 14.5°, **2a** = 17.9°) and shorter Pd…Pd separation of **2a** allow for a short intramolecular contact in **2a** (C22…C1 = 3.400 Å) and intradimer aromatic ring centroid distances (N1,C1-C5 centroid…C18-C23 centroid distance = 3.80 Å, N2,C13-C17 centroid…C6-C11 centroid distance = 3.84 Å) consistent with π-π stacking interactions described previously.[37]

Notable intermolecular features are also present in the structures of **2a** and **6a**. Both structures pack as pairs of intramolecular dimers (Fig S12 & S13). Two nearest intramolecular dimers are related by inversion, with short interdimer Pd…Pd distances of 3.3606(6) Å and 3.4115(7) Å for **2a** and **6a**, respectively. The packing geometry prevents significant intermolecular π overlap of the ppy ligand moieties in both structures (shortest intermolecular pyridine…pyridine and pyridine...phenyl ring centroid distances = 6.88, 5.31 Å (**2a**), 7.41, 5.43 Å (**6a**)). However, the distances between neighboring interdimer parallel least-squares planes (atoms of coordination Pd sphere; **2a**, 3.16 Å; **6a**, 3.12 Å) as well as the Pd1-Pd2…Pd2 angles

(**2a**, 167.16(2)°; **6a**, 170.47(1)°) suggests these interdimer interactions are important contributions to the packing in **2a** and **6a**. Each pair of dimers has neighboring dimer pairs at further distances that pack with geometry for minimal ppy moiety π overlap (shortest intermolecular pyridine…pyridine and pyridine…phenyl centroid distances = 4.12, 4.90 Å (**2a**); 5.05, 4.02 Å (**6a**)) indicative of significant lateral π slippage with longer Pd…Pd separations (**2a**, 5.7143(9) Å; **6a**, 5.1003(8) Å).

[Pd(C^N)([9]aneS$_2$O)](PF$_6$) complexes

Anisotropic thermal displacement ellipsoid diagrams are presented for **1b** and **4b** in Fig. 5. In each of the related structures **1b**, **2b**, **4b*CH$_3$NO$_2$**, and **4b*CH$_3$CN**, and **5b*CH$_3$NO$_2$**, the molecular cation consists of a square planar Pd(II) center with a chelating cyclometallating ligand and an *exodentate* bound [9]aneS$_2$O ligand with two typical length Pd-S bonds. As observed in related structures of cyclometallated Pd [9]aneS$_3$ complexes, the Pd-N bonds are consistently slightly shorter than the Pd-C bonds. Likewise, the Pd-S bond *trans* to the Pd-N bond is about 0.1 Å shorter than the Pd-S *trans* to the Pd-C bond. The aldehyde functional group of the ligand in **2b** is oriented nearly in the ppy plane (O2-C18-C15-C16 = 176.5(5)°) pointed away from the Pd. Only the *exodentate* binding motif is observed for the [9]aneS$_2$O complexes of this study. This *exodentate* bonding is clear from the intramolecular Pd…O distances, which vary only slightly across this series (3.48-3.53 Å, Table 2). The oxygen atom of [9]aneS$_2$O is beyond van der Waals radii contact and oriented in a manner that precludes intramolecular interaction with Pd.

Table 1. Crystal Data, Data Collection, and Refinement Parameters for [Pd(ppy)([9]aneS$_2$O)](PF$_6$) (1b), [Pd(ppyCHO)([9]aneS$_2$O)](PF$_6$) (2b), [Pd(btp)([9]aneS$_2$O)](PF$_6$) (4b), and [Pd(pbt)([9]aneS$_2$O)](PF$_6$) (5b)

Compound	**1b**	**2b**	**4b*CH$_3$NO$_2$**	**4b*CH$_3$CN**	**5b *CH$_3$NO$_2$**
Formula	$C_{17}H_{20}$	$C_{18}H_{20}F_6NO_2PPdS_2$	$C_{19}H_{20}F_6NOPdS_3$ *CH_3NO_2	$C_{19}H_{20}F_6NOPdS_3$ *CH_3CN	$C_{19}H_{20}F_6NOPdS_3$ *CH_3NO_2
Lattice type	Monoclinic	Monoclinic	Triclinic	Triclinic	Triclinic
Space group	$P2_1/c$	$P2_1/c$	P-1	P-1	P-1
a, Å	14.9321(11)	14.3588(14)	8.1573(8)	8.200(3)	8.3654(11)
b, Å	11.8841(9)	12.2238(13)	11.5199(12)	11.574(5)	11.5711(15)
c, Å	12.3550(9)	13.3861(14)	14.1783(14)	13.934(5)	14.3794(19)
α, deg	90	90	80.646(6)	81.388(6)	95.561(7)
β, deg	110.699(8)	114.020(8)	73.894(5)	73.532(5)	105.629(7)
γ, deg	90	90	77.935(6)	79.026(6)	106.146(8)
V, Å^3	2050.9(3)	2146.1(4)	1244.0(2)	1238.5(8)	1265.1(3)
Z	4	4	2	2	2
Fwt., g mol^{-1}	569.84	597.85	686.96	666.97	686.96
D_c, Mg m^{-3}	1.845	1.850	1.834	1.788	1.803
Total refls.	20724	21879	13061	12954	12850
Unique refls.	4698 (R_{int}=0.029)	4926 (R_{int}=0.052)	5700 (R_{int}=0.025)	5653 (R_{int}=0.023)	5752 (R_{int}=0.035)
Data, rest., param.	4698 / 0 / 262	4926 / 21 / 302	5700 / 0 / 326	5653 / 0 / 317	5752 / 47 / 381
R_1, wR_2 ($I > 2\sigma(I)$)	0.0325, 0.0682	0.0473, 0.1073	0.0326, 0.0818	0.0292, 0.0714	0.0729, 0.1449
R_1, wR_2 (all data)	0.0416 / 0.0717	0.0674, 0.1170	0.0371, 0.0842	0.0328, 0.732	0.0843, 0.1495
Goodness-of-fit (F^2)	1.038	1.037	1.080	1.075	1.185

While [9]aneS_2O has been shown to bind in both *endo* and *exo* fashion, depending on the metal, within Pd complexes, only one example of *endodentate* [9]aneS_2O is reported (Pd([9]aneS_2O)Cl_2).14 One could envision either intramolecular or intermolecular factors favoring *exo* or *endo* bonding of [9]aneS_2O. Intramolecular features favoring *exodentate* bonding could include the macrocycle conformation. The bonded [9]aneS_2O macrocycle conformation observed in each of these structures is the [234] conformer, in the modified Dale notation.[38] The same conformation is observed in both the *endo* and *exo* polymorphs of Pd([9]aneS_2O)Cl_2 as well as the homoleptic complex [Pd([9]ane$S_2O)_2$]$(PF_6)_2$[18] (Table 2). Previous studies, using molecular mechanics calculations, have shown that strain energies for [9]aneS_3 complexes are significantly less for the [333] conformer compared with the [234] conformer.[39] The only [9]aneS_2O Pd complexes reported outside this study also exhibit the [234] conformer. This is consistent with smaller calculated conformer strain energy differences for mixed donor macrocycles (such as [9]aneS_2N) compared with macrocycles of a single donor atom type.[39] The lower symmetry [234] conformation may be favored for lower symmetry mixed donor macrocycles (such as [9]aneS_2O) as the C-O-C angle of [9]aneS_2O (~117°) is considerably larger than the C-S-C angle (101-105°), and a more asymmetric binding conformation can accommodate these significant angle differences. Another contribution that may help favor the *exodentate* conformation lies in a persistent short intramacrocyclic contact. A short [9]aneS_2O oxygen…H-C(position 5) contact (2.30-2.49 Å) less than van der Waals radii sum (average = -0.35 Å) is found in each of the structures of this study (Fig. S15). While this C-H…O interaction is not expected to be a strong intramolecular feature, this contact could contribute to the stability of the *exodentate* conformation observed crystallographically. This

interaction is also observed in the X-ray structures of the *exo* forms of M([9]aneS_2O)Cl_2 and [M([9]aneS_2O)$_2$]$(PF_6)_2$, (M=Pd, Pt)).

Intermolecular features were examined to identify potential influence on the preferred *exodentate* [9]aneS_2O bonding. The π-stacking interactions observed are discussed here in the context of formerly described motifs.[34] The structure of **1b** packs as isolated π-dimers in an out-out motif with a ppy ligand π-π parallel least-squares plane separation of 3.38 Å, with no intermolecular contacts involving oxygen (Fig. S16). The packing of **2b** differs in that while π dimers are present with significant π overlap and close parallel separation (3.32 Å), each dimer has four additional nearly parallel dimers with close aldehyde…pyridine π contacts (C18…O11 3.28 Å) (Fig. S17). The oxygen of [9]aneS_2O in **2b** also has a short intermolecular contacts with a C-H bond of a nearby bonded [9]aneS_2O (O1..H6Aa = 2.67 Å). The aldehyde oxygen of the ppyCHO also has a short intermolecular contact with a C-H of nearby bonded [9]aneS_2O (O2..H5B = 2.63 Å). The structure of **4b*CH_3NO_2** has no [9]aneS_2O intermolecular oxygen contacts, and packs in an slipped infinite π-stack with an alternating out-out/in-in motif, at interplanar separations of 3.39 Å (out-out) and 3.46 Å (in-in) (Fig. S18). The acetonitrile solvate **4b*CH_3CN** has similar intermolecular oxygen…hydrogen contact as **2b** (2.64 Å), and a π-stacking motif nearly identical to the nitromethane solvate structure (3.40 Å out-out, 3.46 Å in-in) (Fig. S18). The structure of the pbt analog **5b*CH_3NO_2** is very similar to that of **4b*CH_3CN** with the same π-stacking motif (3.39 Å out-out, 3.60 Å in-in) and intermolecular oxygen…hydrogen contact (2.55 Å) (Fig. S19). Any direct relationship between the cyclometallated ligand and the resulting π-stacking motif adopted is unclear. While the anion remains the same across this series of structures, the presence or absence of solvent (none,

CH_3NO_2, CH_3CN) and temperature effects (173K for **1b**, **4b*CH_3NO_2**, **4b*CH_3CN**, **5b*CH_3NO_2**; 293K for **2b**) could play a role in the observed solid-state π-stacking motif. While π-stacking is found in all these solid-state structures, neither π–interactions nor the intermolecular C-H...O interactions found in some (not all) of the structures in this series are not expected to strongly influence *exo*/*endo* preferences of this series, as they are not particularly short.

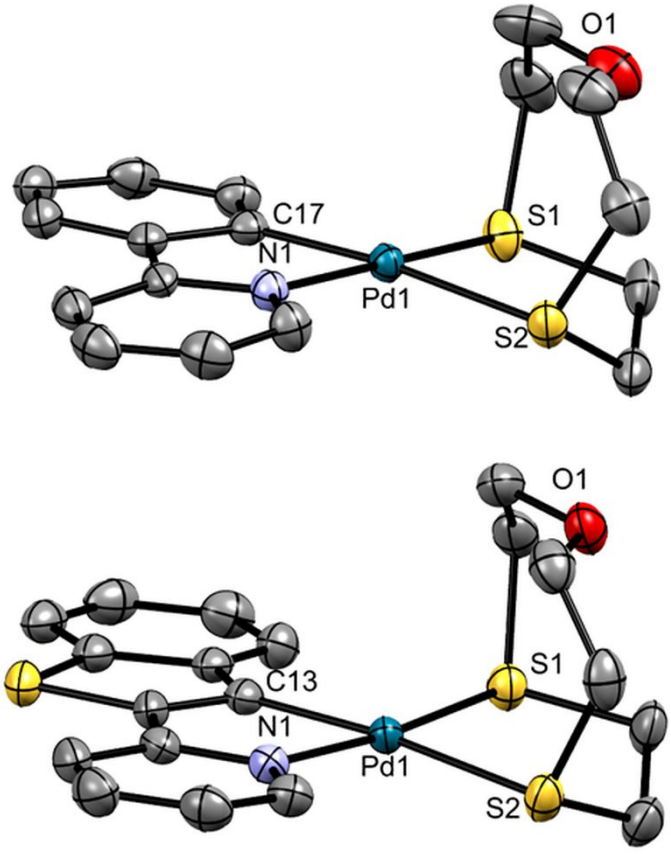

Figure 5. Thermal ellipsoid perspective of the cation of [Pd(ppy)([9]aneS_2O)](PF_6) (1b, top) and [Pd(btp)([9]aneS_2O)](PF_6) (4b*CH_3NO_2, bottom) (50% probability, H atoms, anions, and solvent omitted for clarity).

Table 2. Selected Intramolecular Distances (Å), van der Waals radii Sum Comparisons, and Macrocycle Ligand Binding Descriptors for Related Heteroleptic Pd Complexes of [9]aneS_2O and [9]aneS_3

Coligand(s)	[9]aneS_2O					[9]aneS_3				
	Pd….O distance	vdW radii# sum – dist.	*Exo* or *Endo*	macrocycle conformation	Ref.	Pd….S distance	vdW radii sum – dist.	*Exo* or *Endo*	macrocycle conformation	Ref.
ppy	3.530(3)	+0.38	*exo*	[234]	*	2.871(1)	-0.56	*endo*	[333]	1
ppyCHO	3.476(5)	+0.33	*exo*	[234]	*	2.888(1)	-0.54	*endo*	[333]	*
btp	3.481(2)	+0.33	*exo*	[234]	*[a]	2.909(2)	-0.52	*endo*	[333]	2
btp	3.454(2)	+0.30	*exo*	[234]	*[b]					
pbt	3.487(5)	+0.34	*exo*	[234]	*	2.894(2)	-0.54	*endo*	[333]	2
bzq	NA	NA	NA	NA	NA	3.007(1)	-0.42	*endo*	[234], [333]	1
2Cl	2.957(1)	-0.19	*endo*	[234]	3	3.140(2)	-0.29	*endo*	[234]	4
2Cl	3.406(2)	+0.19	*exo*	[234]	3					
homoleptic	3.379(5)	+0.23	*exo, exo*	[234], [234]	5	2.957(2)	-0.47	*endo, endo*	[333], [333]	6

*This study. # van der Waals radii values S = 1.8 Å, Pd = 1.63 Å, O = 1.52 Å obtained from A. Bondi, *J. Phys. Chem.,* 1964, **68**, 441-452. NA = not available. [a] CH_3NO_2 solvate [b] CH_3CN solvate [1] D.E. Janzen, D.G. VanDerveer, L.F. Mehne, D.A. da Silva Filho, J.-L. Bredas and G.J. Grant, *Dalton Trans.*, 2008, **14**, 1872-1882. [2] D.E. Janzen, M.A. Bruening, C.A. Sutton and A.R. Sharma, *J. Organomet. Chem.*, 2015, **777**, 31-41. [3] J.P. Tidey, H.L.S. Wong, J.McMaster, M.Schröder and A.J. Blake, *Acta Cryst.*, 2016, **B72**, 357-371 (*endo* REFCODE -NONWES60, *exo* REFCODE: NONWES68, both at 240K). [4] A.J. Blake, A.J. Holder, Y.V. Roberts and M. Schröder, *Acta Cryst.*, 1988, **C44**, 360-361. [5] G.J. Grant, D.F. Galas, M.W. Jones, K.D. Loveday, W.T. Pennington, G.L. Schimek, C.T.Eagle and D.G. VanDerveer, *Inorg. Chem.*, 1998, **37**, 5299-5305. [6] K.Wieghardt, H.-J. Küppers, E. Raabe and C. Krüger, *Angew. Chem.,Int. Ed.*, 1986, **25**, 1101-1103.

Structure of [Pd(ppyCHO)([9]aneS$_3$)](PF$_6$) (2c)

A careful comparison of the structure of **2c** with the analogous [9]aneS$_2$O structure of **2b** gives insight into structural effects induced by the macrocyclic ligand, as neither structure contains solvent, both have the same anion, and crystal growth conditions were identical. The molecular cation of **2c** consists of a square pyramidal Pd(II) center with a chelating cyclometallating ligand; an *endodentate* bound [9]aneS$_3$ ligand with two typical Pd-S bonds, and a longer intramolecular Pd…S axial interaction (2.888(1) Å). Anisotropic thermal displacement ellipsoid diagrams are presented for **2b** and **2c** in Fig. 6. The aldehyde functional group of the ligand in **2c** is oriented nearly in the ppy plane (O2-C18-C15-C14 = 178.0(3)°) but is pointed toward the Pd. Most intramolecular features of **2b** and **2c**, including the Pd-C, Pd-N, and Pd-S bonds, exhibit remarkably similar metrics such as the pattern and magnitudes of bond lengths. However, the structure of **2c** shows a displacement of the Pd of 0.14 Å from the plane formed by the coordinated atoms in the direction of the axial Pd…S interaction, while **2b** shows a smaller such distortion (0.04 Å). The *endodentate* axial sulfur atom in **2c** lies 0.54 Å closer to Pd than the Pd/S van der Waals radii sum and in an orientation for favorable orbital overlap with a Pd dz^2 orbital. The Pd…S axial interaction distance falls squarely in the range observed for similar Pd cyclometallated complexes (Table 2). This *endodentate* bonding of [9]aneS$_3$ is consistent with the appearance of a fluxional [9]aneS$_3$ observed in solution by ^{1}H and ^{13}C NMR of **2c** and the observation that essentially all Pd structures involving [9]aneS$_3$ (92 structures[40]) demonstrate *endodentate* bonding. The single report of an *exodentate* bonded [9]aneS$_3$ at Pd for the complex [Pd([9]aneS$_3$)(κ^1-O$_2$CCH$_3$)$_2$] surprisingly yields an NMR consistent with fluxional *endodentate* [9]aneS$_3$ in room temperature CD$_3$NO$_2$ solution.[41] While specific intermolecular packing forces may be the cause for the *exodentate* binding in this specific solid-state structure of

[Pd([9]aneS$_3$)(κ^1-O$_2$CCH$_3$)$_2$], the barrier to *endo/exo* conversion must not be large for facile access of both bonding modes.

The intermolecular features of **2c** are significantly different from those of **2b**. The structure of **2c** packs as isolated π-dimers with an in-in motif and an intradimer interplanar separation of 3.37 Å (Fig. S20). While nearby dimers also stack in a parallel layered fashion (interdimer planar separation of 2.92 Å), displacement of neighboring ppy ligands prevents infinite π-stacking. Also, within each inversion-related π-dimer there is a pair of close CH…S contacts at 2.89 Å involving the axial sulfur and C-H bond of the ppyCHO ligand.

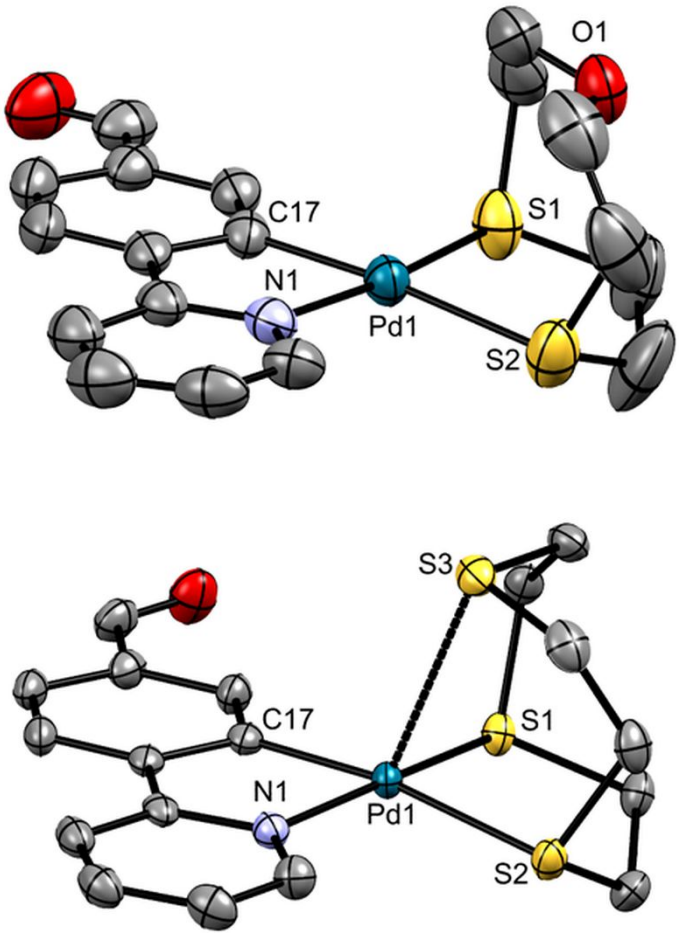

Figure 6. Thermal ellipsoid perspective of the cation of [Pd(ppyCHO)([9]aneS$_2$O)](PF$_6$) (2b, top) and [Pd(ppyCHO)([9]aneS$_3$)](PF$_6$) (2c, bottom) (50% probability, H atoms, and anions omitted for clarity). Larger thermal parameters for 2b are due to 293K data collection (2c collected at 173K).

DFT Calculations

DFT calculations were carried out on **4b** to help understand features of the electronic structure and the low-lying excited states of this compound. Comparison of the crystal structure geometry of the cation of **4b** with that of the geometry minimized structure demonstrates they are remarkably similar (Figure S21, RMS deviation of 25 atom coordinate pairs = 0.131). The

frontier orbitals of **4b** from DFT calculation were examined to better understand the electronic structure of the molecular cation. The calculated HOMO and LUMO of **4b** are shown in Fig. 7.

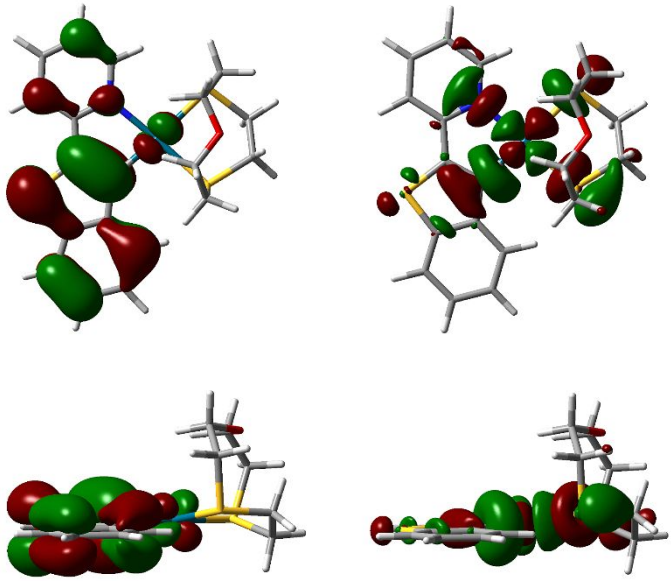

Figure 7. DFT calculated HOMO (left column) and LUMO (right column), of complex 4b, [Pd(btp)([9]aneS$_2$O)]$^+$. Upper perspective perpendicular to coordination plane, lower perspective parallel to coordination plane. Plots at isovalue 0.03, density 0.0004.

The HOMO of **4b** has orbital contributions from the d_{xz} orbital of Pd (along C-Pd-S bonding vector) as well pπ btp ligand orbitals. The LUMO of **4b** consists mainly of the σ bonding framework of the Pd coordination sphere with contributions from bonded N, C, and S atoms with the $d_{x^2-y^2}$ orbital at Pd. As expected from the bonded *exodentate* geometry of the [9]aneS$_2$O ligand, no significant interaction of the oxygen atom of the ligand with the Pd orbitals is present. This is in stark contrast with previous calculations on the related [Pd(ppy)([9]aneS$_3$)]$^+$ complex[9] where the Pd d_{z^2} orbital and a p orbital of the axial sulfur of the endodentate [9]aneS$_3$ showed significant orbital contributions in the HOMO. The LUMO, however, is remarkably similar for both **4b** and [Pd(ppy)([9]aneS$_3$)]$^+$.

In an effort to help explain the variable temperature NMR results for **2b**, free energies were calculated for both *endo* and *exo* forms of the related complex **4b**. These *endo* and *exo* bonding mode geometries were then used in a calculation to determine a transition state geometry and energy barrier to conversion between these complexes (Fig. 8). DFT calculations on related systems have been used previously to study the relative energies of energies of *endo* and *exodentate* bonding modes of 9-membered tridentate macrocycles and the effects of axial donor atoms.[42,43]

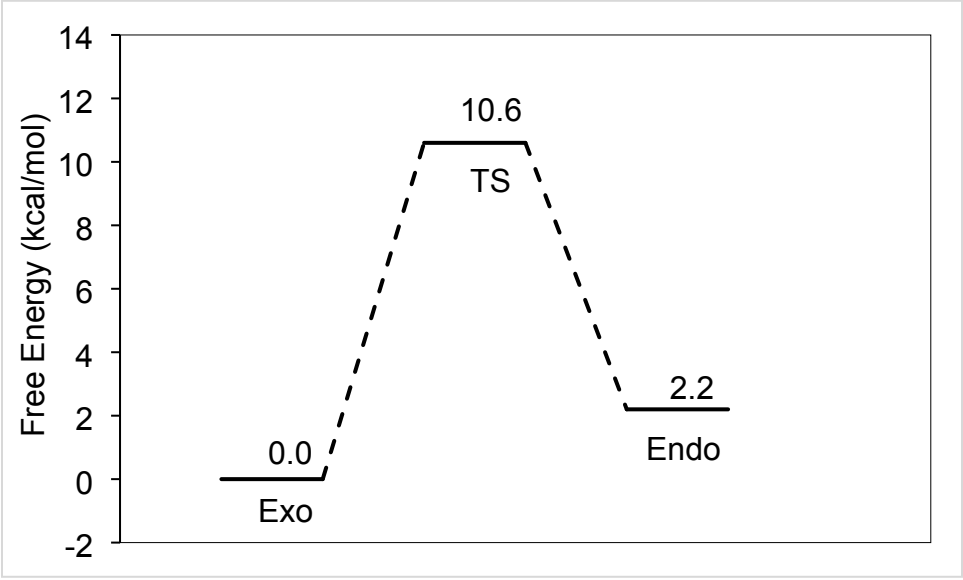

Figure 8. Calculated free energy diagram of *endo* and *exo* bonding modes of [Pd(btp)([9]aneS$_2$O)]$^+$ (4b).

The thermodynamically more stable *exo* form is consistent with the obtained X-ray structure of **4b** (*exodentate*). The *endo* conformer, however, is less stable by only 2.2 kcal/mol. This difference in calculated energies is reversed in a study of the *endo*/*exo* forms of Pd([9]aneS$_2$O)Cl$_2$ (*endo* 4.6 kcal/mol lower in energy than *exo*).[43] The calculated barrier to interconversion from *exo*-**4b** to *endo*-**4b**, 10.6 kcal/mol, suggests that a significant population of the less stable *endo* form is reasonable near room temperature. The significant presence of both

endo and *exo* forms of **4b** and a relatively low barrier to interconversion is also consistent with previous work on the related compound Pd([9]aneS$_2$O)Cl$_2$, for which X-ray crystal structures were obtained for both *endo* and *exo* forms. In this crystallographic study of Pd([9]aneS$_2$O)Cl$_2$, the *endo* form was favored at lower crystal growth temperatures, had a higher density, and calculations of total and cohesive energies supported the *endo* form as more stable than the *exo* form.19 An explanation for this reversal in favored bonding mode for **4b** lies in the coligand donor/acceptor properties. As the benzothienylpyridine carbanion of **4b** is both a strong σ-donor and π-acceptor, electron density at the metal is enhanced relative to the chloride π-donor ligands of Pd([9]aneS$_2$O)Cl$_2$. This could account for the increased stability of the *endo* form for the more electron poor Pd center of Pd([9]aneS$_2$O)Cl$_2$ where the axial oxygen donor supplies electron density in the *endo* form at a distance appropriate for orbital overlap with the metal. Related work[31,44] on Pt, suggests that increased electron density at the metal provided by coligands leads to longer axial d^8 metal…sulfur distances in [9]aneS$_3$ complexes. Longer Pd…O distances will by definition diminish the electron donation capacity of the axial oxygen. In the complex **4b**, the cyclometallating btp ligand provides an electron-rich metal center that does not significantly effect the stability of an *exo* form (as no close oxygen interaction is possible) but rather diminishes the need for donation by an *endo* oxygen, resulting in less stability of the *endo* bonding mode.

In an attempt to quantify any Pd…O interactions in the *endo* and *exo* forms of **4b**, a Natural Bond Order Analysis[45] was carried out on each form. Using the natural population analysis[46], calculated atomic charges (Table S2) on Pd are positive values (~0.51 au) with smaller positive values for [9]aneS$_2$O sulfur atoms (~0.35 au). Ligated C19 bears a small negative charge (~ -0.05 au), while nitrogen (~ -0.48 au) and oxygen (~ -0.62 au) bear a greater

negative charge. A close comparison of changes in atomic charges between *endo* and *exo* forms reveals small changes in atomic charge involving oxygen (*endo* = -0.612 au; *exo* -0.634 au) while the ligated atoms show little change. The difference between the Pd/O charges for the *endo* form (1.13 au) is similar to the difference for the *exo* form (1.14 au), suggesting little to no interaction. If significant electron donation of the oxygen through a lone pair to the Pd atom was present in the *endo* form, less negative charge on the oxygen atom and less positive charge at the Pd might be observed. In the case of calculations on the *endo* and *exo* forms of Pd([9]aneS-$_2$O)Cl$_2$, a larger decrease in charge difference was observed in the *endo* form than the *exo* form compared with the atomic charges in our system.[43] Results obtained from calculating atomic charges using the CHELPG scheme (CHarges from ELectrostatic Potentials using a Grid based method) showed similar effects, with no strong evidence for charge transfer in the *endo* form.

Through atomic charges do not indicate significant interactions in the *endo* form of **4b**, we looked for evidence of an axial interaction in the second-order perturbative estimates of 'donor-acceptor' interactions in the NBO basis. A few very weak interactions were found involving filled oxygen Lewis-type lone pair orbitals acting as donors to empty antibonding non-Lewis Pd orbitals (Table S3). No such donor-acceptor interactions involving oxygen lone pairs and Pd orbitals are present in the *exo* form. As a control, we compared these results to the 9[ane]S$_3$ analogue, [Pd(btp)(9[ane]S$_3$)]$^+$. A significant interaction (8.5 kcal/mol) is found here between the axial sulfur and Pd in this complex where the 9[ane]S$_3$ binds in an *endodentate* fashion. A persistent axial Pd…S interaction in [Pd(btp)(9[ane]S$_3$)]$^+$ is consistent with exclusive fluxional endodentate 9[ane]S$_3$ NMR results of this complex, and a short Pd…S axial distance in the crystal structure.

The lack (*exo*) or presence (*endo*) of an axial oxygen is not likely the sole contributor to the stability of these two forms. Others factors need to be considered. There is a possibility that ring conformers preferred for *endodentate* and *exodentate* coordination may differ significantly, leading to a metal complex macrocycle preference for conformation solely based on the ligand. Previously reported DFT calculations performed suggest the unligated [9]aneS_2O *exodentate* form is lower in energy than the *endodentate* geometry by 3.5 kcal/mol.[43] While a barrier for interconversion of these geometries was not calculated, this difference in *endo/exo* stabilities is similar to the difference calculated for the conformers of **4b**. Even within *endodentate* and *exodentate* metal bonding modes, several common conformers differing by arrangements of gauche torsions are observed amongst complexes of [9]aneS_3 and [9]aneS_2O, including the [234], [333], and [12222] conformers, which also differ in energy. X-ray structural data for cyclometallated Pd complexes suggests that [9]aneS_3 is the preferred [333] *endodentate* conformation, while [234] is most common for *exodentate* [9]aneS_2O. Solvent incorporation in a crystal structure or intermolecular solid-state packing forces could also influence the stability of *endodentate* vs *exodentate* ligand binding. In the case of the two solvatomorphs of **4b**, the solvent seems to play a negligible role as the *exodentate* bonding mode and [234] conformer are the same for both structures, and intermolecular packing is nearly identical.

The transition state geometry calculated for the *exo/endo* bonding interconversion of **4b** is shown in Fig. 9, overlapped with the coordinates of the energy minimized calculated *endo* and *exo* bonding geometries. The overall geometry at Pd and the btp ligand is virtually unchanged. The calculated intramolecular Pd…O distances (*exo* = 3.65 Å, *endo* = 2.93 Å) agree well with experimental values for *exo*-**4b** (3.481(2) Å, 3.454(2) Å) and the Pd([9]aneS_2O)Cl_2 *endo* polymorph (2.957(1) Å). The transition state geometry indicates a swing of the oxygen atom

through the cavity of the [9]aneS_2O macrocycle, achieving a shorter Pd…O distance in the transition state (2.83Å) than in the *endo* form, rather than outside and away from the Pd. This relatively minor geometry change accompanying the *endo*/*exo* interconversion is consistent with a small entropy change proposed to help explain the dynamic NMR results. Also, comparison of simple van der Waals surface volume calculations of these *exo*, transition state, and *endo* forms of **4b** are consistent with small overall geometric changes (*endo* = 457.6 $Å^3$, t.s. = 468.4 $Å^3$, *exo* 458.1 $Å^3$). Accompanying this large change in the Pd…O distance is a significant bond angle change at the oxygen. The C-O-C bond angle changes from 117.8° in the *exo* form, to 124.7° in the transition state, and settling at 116.7° in the *endo* form, with negligible change in the C-O bond lengths. This may hint at why dynamic *endo/exo* conversion has not been observed for [9]aneS_3. The C-S bonds in [9]aneS_3 are considerably longer compared with C-O bonds in [9]aneS_2O (average C-S length 1.80 Å; average C-O length = 1.42 Å). If a similar mechanism is invoked in a [9]aneS_3 d^8 metal complex, the swing of the axial S through the macrocycle ring could yield a prohibitive barrier for interconversion as the sulfur would pass even closer to the metal. Alternately, the axial metal….S interaction is simply stronger (than metal…O), and regardless of barrier to interconversion, the *endodentate* conformer is highly favored through sulfur lone pair overlap with the d_z^2 metal orbital. Further computational studies are underway to better understand the strength and nature of these types of axial interactions.

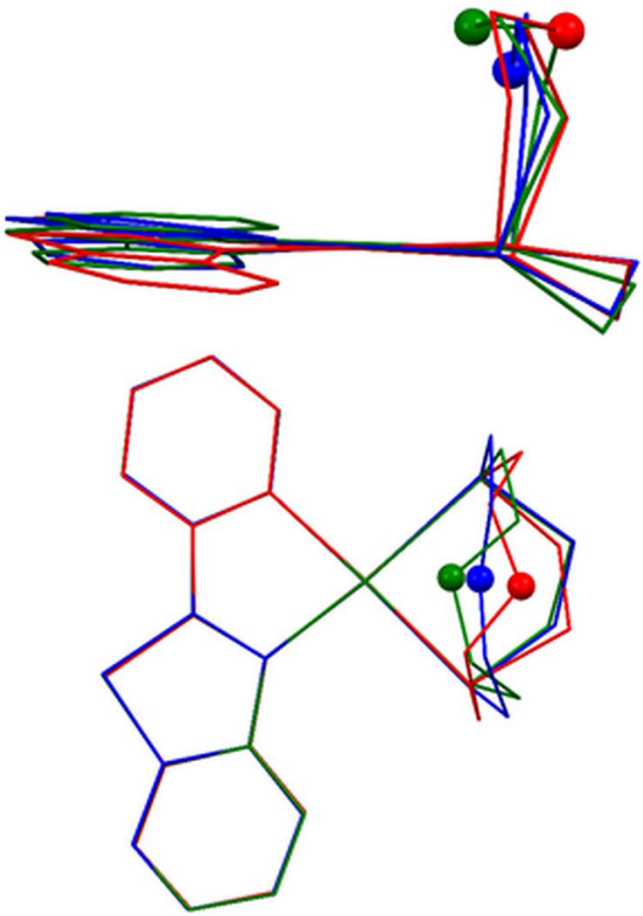

Figure 9. Overlap of DFT calculated geometries of *endo* (green), *exo* (red), and transition state (blue) of [Pd(btp)([9]aneS$_2$O)](PF$_6$) (4b). Oxygen atoms of [9]aneS$_2$O ligands shown as spheres. Above: side view of changes in [9]aneS$_2$O geometry. Below: view perpendicular to the coordination plane.

Conclusions

A series of cyclometallated complexes of Pd(II) with [9]aneS$_2$O were prepared in a synthetic fashion similar to their [9]aneS$_3$ derivatives. Marked differences, however,, are observed in their solution behavior and solid-state structures. NMR spectra of these [9]aneS$_2$O complexes indicate the presence of both *exodentate* and *endodentate* bonding modes of this macrocycle. X-

ray crystal structures demonstrate only *exodentate* bonding of [9]aneS_2O with no Pd…O axial interactions in the solid-state. Only weak intermolecular π-stacking interactions dominate the packing in the crystal structures. DFT calculations support the NMR interpretation of *endo*/*exo* interconversion, the crystallography results suggesting greater stability of the *exodentate* bonding mode, and provide evidence for weak Pd…O bonding in the *endodentate* form of [9]aneS_2O. Likely contributors to the differences between related [9]aneS_3 and [9]aneS_2O cyclometallated Pd(II) complexes include ring conformer bonding preferences, relative energy ordering of free ligand *endo* and *exo* forms, other intramolecular intramacrocyclic interactions, and the strength of the donor-acceptor interaction of S vs O with Pd.

Experimental

Materials and Measurements

All materials were used as received. The ligands [9]aneS_3, btp, pbt, as well as NH_4PF_6 were purchased from Sigma-Aldrich. The ligand [9]aneS_2O was prepared as previously reported.[14] Palladium(II) acetate was purchased from Strem. The ligands fpp, bzq, and ppyCHO were purchased from TCI. Cyclometallated acetate dimers used in the preparation of **1b**, **3b**, **4b**, and **5b** were prepared as previously reported.[8] $[Pd(ppy)Cl]_2$ was prepared by the reported method.[47] All synthetic manipulations were carried out in air. Elemental analyses were performed by Atlantic Microlab. Fourier transform IR spectra were obtained for solid samples using a Perkin Elmer Spectrum One FTIR with diamond ATR accessory. Proton and carbon-13 NMR spectra were obtained on a JEOL 400 MHz NMR spectrometer using residual solvent for both the deuterium lock and reference. Variable temperature measurements were performed using a JEOL temperature-controlled probe. Samples were held at each temperature for 10 min prior to

acquisition of each spectrum. After spectra were collected at the lowest and highest temperatures recorded, room temperature spectra were recollected and compared with the initial room temperature spectra to ensure equilibrium NMR measurements were acquired. Mass spectra were acquired using a Thermo LCQ Fleet ESI–MS.

DFT Calculations

All quantum mechanical calculations were performed using the Gaussian 09 program suite.[48] Density functional theory calculations were performed using the B3LYP functional.[49,50] The Hay and Wadl effective core potential basis set (termed LANL2DZ[51] in Gaussian) was used to describe the Pd atoms whereas the 6-311+G(d,p) was used for the remaining atoms (except for the first geometry minimization steps, as specified below). All DFT calculations were performed using PCM (Polarizable Continuum Model)[52], choosing acetonitrile as the implicit solvent. DFT calculations were performed using X-ray structural data as a starting point for geometry minimizations and excluded the PF_6^- anion in all calculations. Geometry minimizations were performed by first minimizing using LANL2DZ/6-31G* basis set with ”fine” integration grid, followed by minimization with LANL2DZ/6-311+G(d,p) with ”ultrafine” integration grid, followed by a more accurate minimization, with new calculation of force constants at every step, through the ”calcall” keyword. CHELPG[53] charges were calculated using Gaussian09, taking Bondi radii as the Van der Waals radii for all atoms: H 1.20 pm, O 1.52 pm, C 1.70 pm, S 1.80 pm, N 1.55 pm, Pd 1.63. NBO charges were obtained using standalone NBO 7.0,[54] from input generated by Gaussian09 through its embedded NBO version 3.1. For thermochemical calculations of **4b**, only singlet species of overall charge +1 were considered. The optimized geometry of *exodentate* $[Pd([9]aneS_2O)(btp)]^+$ using acetonitrile solvent (using the Polarizable Continuum Model) was calculated with the X-ray structural data obtained as a starting point. For

the *endodentate* form, the optimized geometry (using acetonitrile solvent) was obtained by starting with the X-ray structural coordinates of $[Pd([9]aneS_3)(btp)]^+$ with the axial sulfur reassigned as oxygen (coordinates obtained from a previously collected published structure[8]). A transition state between these *endo* and *exo* forms was obtained using the Synchronous Transit-Guided Quasi-Newton method,[55] followed by a transition state search using the opt=(ts,calcall) keywords.[56] The transition state geometry was verified by the presence of a single imaginary frequency. Calculated free energies are reported as the sum of electronic and thermal free energies. The program Multiwfn[57] was used to calculate the molecular van der Waals volume.

X-ray Crystallography

Tables 1 and S1 contain crystal data, collection parameters, and refinement criteria for the crystal structures of **1b**, **2b**, **4b*CH_3CN, 4b*CH_3NO_2, 5b*CH_3NO_2** and **2a, 6a, 2c,** respectively. Crystals were mounted on the tip of MiTeGen micromount and X-ray intensity data were measured at low temperature using an Oxford Cryosystems desktop cooler[58] (173(2)K for all structures except **2b** (293(2)K)) with graphite monochromated Mo Kα radiation (λ = 0.71073 Å) on a Rigaku XtaLAB mini diffractometer.[59] A preliminary set of cell constants was calculated from reflections harvested from 12 frames. A randomly oriented region of reciprocal space was surveyed to the extent of one sphere and to a resolution of at least 0.80Å. Three major sections of frames were collected with 1.0° steps in ω at three different φ settings. The intensity data were corrected for absorption[60] and decay using CrystalClear.[59] Final cell constants were calculated from the xyz centroids of strong reflections from the actual data collection after integration using CrystalClear.

Each structure was solved and refined using SHELXL-2013[61] within the CrystalStructure program suite.[62] A direct-methods solution was calculated that provided most of the non-hydrogen atoms from the E-map. Full-matrix least-squares/difference Fourier cycles were performed that located the remaining non-hydrogen atoms. All non-hydrogen atoms were refined with anisotropic displacement parameters. All of the hydrogen atoms in each structure were placed in ideal positions and refined as riding atoms with relative isotropic displacement parameters.

Crystals of **2a** and **6a** were grown by vapor diffusion of hexanes into a concentrated CH_2Cl_2 solution at room temperature. Both structures **2a** and **6a** consist of one entire dimer in the asymmetric unit, with all atoms on general positions. One CF_3 group of the dimer in **6a** was modeled with positional disorder over two positions differing by rotation around the bond C24-C21 with freely refined occupancies of 66/34.

Crystals of **1b**, **2b**, **4b*CH_3NO_2**, and **5b*CH_3NO_2** were grown by vapor diffusion of diethyl ether into concentrated CH_3NO_2 solutions at room temperature. Crystals of **4b*CH_3CN** were grown by slow evaporation of an CH_3CN solution at room temperature. In the structures of **1b** and **2b**, the asymmetric unit is composed one cation/anion pair, with all atoms on general positions. The structures of **4b*CH_3NO_2**, **4b*CH_3CN**, and **5b*CH_3NO_2** similarly contain one cation/anion pair and one solvent molecule in the asymmetric unit, with all atoms on general positions. In the structure of **2b**, one PF_6^- anion was modeled with positional disorder over two locations with freely refined occupancies of 37/63 and pairwise thermal parameter constraints. Disorder in the structure of **5b** was modeled for Pd and the entire pbt ligand over two unique sets of positions in the same plane that involve swapping of ligated rings coordinated to the metal. The final model freely refined with occupancies of 79/21 for the two sets of Pd/pbt positions

using the SAME restraint and accompanied by appropriate pairwise thermal parameter constraints. Numerous lower quality X-ray data sets were collected on crystals grown of **5b** at both room temperature, and 5°C and all showed evidence of this disorder.

Crystals of **2c*CH_3NO_2** were grown by vapor diffusion of diethyl ether into a concentrated CH_3NO_2 solution at room temperature. The asymmetric unit of **2c** is composed one cation/anion pair and one solvent molecule, with all atoms on general positions.

Syntheses of [Pd(C^N)(μ-O_2CCH_3)]$_2$ Complexes

Preparation of [Pd(fpp)(μ-O_2CCH_3)]$_2$ (6a) To a solution of fpp (0.216 g, 0.963 mmol) in CH_2Cl_2 (30 mL) was added solid palladium(II) acetate (0.15 g, 0.6 mmol). The solution was heated at reflux for 12hrs, changing to a bright orange product. The reaction was diluted with CH_2Cl_2 (40mL) and washed with water (2 x 25mL). The CH_2Cl_2 was removed under reduced pressure yielding a bright orange precipitate. The product was recrystallized from CH_2Cl_2/hexanes. Yield: 0.286g, 0.369mmol, 77%. Anal. Calc. for $C_{28}H_{20}F_6N_2O_4Pd_2$: C, 43.38, H, 2.60, N, 3.61. Found: C, 43.39, H, 2.52, N, 3.57. ^{1}H-NMR (400 MHz, CD_2Cl_2, *only major isomer reported): δ = 7.92 (d, J=5.0Hz, 1H), 7.51 (t, J=8.0Hz, 1H), 7.21 (d, J=8.0Hz, 1H), 7.13-6.97 (m, 3H), 6.72 (t, J=8.0 Hz, 1H), 2.25 (s, 3H). ^{19}F-NMR (376MHz, CD_2Cl_2, *indicates minor isomer): δ = -62.98, -63.29*. ATR-IR (diamond): ν/cm^{-1} = 3082, 2929, 2633, 2361, 1608, 1596, 1565, 1487, 1411, 1388, 151, 1316, 1272, 1257, 1235, 1154, 1130, 1116, 1105, 1073, 1034, 902, 897, 823, 814, 775, 746, 739, 734, 718, 685, 661, 648, 624, 544, 466. Isomers present in 90/10 *anti*/*syn* ratio.

Preparation of [Pd(ppyCHO)(μ -O_2CCH_3)]$_2$ (2a) To a solution of 4-(2-pyridyl)benzaldehyde (0.148 g, 0.66 mmol) in CH_2Cl_2 (20 mL) was added solid palladium(II) acetate (0.15 g, 0.67 mmol). The solution was heated at reflux for 6hrs and monitored by TLC (silica gel, CH_2Cl_2), changing to a deep yellow/orange product. The reaction was diluted with CH_2Cl_2 (40mL) and washed with water (2 x 25mL). The CH_2Cl_2 was removed under reduced pressure yielding a light yellow/orange precipitate. The product was recrystallized from CH_2Cl_2/hexanes. Yield: 0.159g, 0.229mmol, 69%. Anal. Calc. for $C_{28}H_{22}F_6N_2O_6Pd_2$: C, 48.37, H, 3.19, N, 4.03. Found: C, 48.27, H, 3.10, N, 3.94. ^{1}H-NMR (400 MHz, CD_2Cl_2, *only major isomer reported): δ = 9.81 (s, 1H), 7.93 (d, J=5.0Hz, 1H), 7.48 (td, J=7.8, 1.4Hz, 1H), 7.33 (dd, J=7.8, 1.4Hz, 1H), 7.29 (s, 1H), 7.22 (d, J=7.8Hz, 1H), 7.08 (d, J=8.0Hz, 1H), 6.67 (td, J=8.0, 0.8Hz, 1H), 2.28 (s, 3H). ^{13}C-NMR (101MHz, CD_2Cl_2, *only major isomer reported): δ = 192.92, 182.76, 163.62, 152.72, 150.68, 139.21, 136.10, 134.26, 125.52, 123.46, 123.43, 119.65, 25.39. ATR-IR (diamond): ν/cm^{-1} = 3075, 2925, 2829, 2730, 2360, 1680, 1605, 1559, 1481, 1345, 1408, 1371, 1343, 1311, 1269, 1236, 1180, 1164, 1109, 1062, 1033, 879, 818, 769, 746, 709, 684, 675, 655, 625, 557, 481. Isomers present in 82/18 *anti*/*syn* ratio.

Syntheses of [Pd(C^N)([9]aneS_2O)](PF_6) Complexes

Preparation of [Pd(ppy)([9]aneS_2O)](PF_6) (1b) To a solution of [Pd(ppy)(Cl)]$_2$ (0.100g, 0.169mmol) in CH_3CN (10mL) was added [9]aneS_2O (0.056g, 0.338mmol) dissolved in CH_3CN (2mL). A pale yellow precipitate formed almost immediately. The reaction mixture was stirred 23 hr at rt. The solvent removed under reduced pressure, and the residue was redissolved in CH_3OH (20mL). Solid NH_4PF_6 (0.0550g, 0.338mmol) was added and precipitate formed gradually. After stirring 24 hours, the pale yellow solid was collected, rinsed with Et_2O

(3x5mL), and dried in vacuo. Yield: 0.121g, 0.218mmol, 65%. Anal. Calc. for $C_{17}H_{20}NPdOS_2PF_6$: C, 35.83, H, 3.54, N, 2.46. Found: C, 35.86, H, 3.42, N, 2.54. ^{1}H-NMR (400 MHz, CD_3NO_2): δ = 8.59 (d, J=5.0Hz, 1H), 8.14 (td, J=8.0, 4.0Hz, 1H), 8.03 (d, J=7.8Hz, 1H), 7.76 (dd, J=7.8, 0.9Hz, 1H), 7.43 (m, 2H), 7.31 (td, J=8.0, 1.2Hz, 1H), 7.22 (td, J=8.0, 1H), 4.57-4.42 (m, 2H), 4.11-3.97 (m, 2H), 3.91-3.42 (m (broad), 4H), 3.41-3.30 (m 2H), 3.29-3.10 (m, 2H). ^{13}C-NMR (101MHz, CD_3NO_2): δ = 160.58, 151.21, 147.06, 142.09, 136.38, 130.55 126.30, 122.24, 120.66, 119.80, 115.61, 73.81-71.01 (2C), 37.98-30.43 (4C). ATR-IR (diamond): ν/cm^{-1} = 3210, 2867, 2360, 1909, 1606, 1577, 1488, 1469, 1437, 1423, 1414, 1297, 1262, 1240, 1172, 1131, 1017, 1004, 885, 828, 754, 733, 663, 649, 629, 615, 555, 503, 478, 463, 455. ESI-MS (rel. ab. %): $[Pd(ppy)([9]aneS_2O)]^+$ m/z 424.08 (100%)

Preparation of [Pd(ppyCHO)([9]aneS$_2$O](PF$_6$) (2b) To a solution of [Pd(ppyCHO)(μ-O_2CCH_3)]$_2$ (0.100g, 0.144mmol) in CH_3CN (25mL) was added [9]aneS$_2$O (0.047g, 0.288mmol) dissolved in CH_3CN (1mL). The reaction mixture was stirred 16 hr at rt. The solvent removed under reduced pressure and the residue was redissolved in CH_3OH (3mL). Solid NH_4PF_6 (0.047g, 0.288mmol) was added and a pale yellow precipitate formed immediately. After stirring 30 min, the solid was collected, rinsed with Et_2O (3x5mL), and dried in vacuo. Yield: 0.150g, 0.251 mmol, 87%. Anal. Calc. for $C_{18}H_{20}NO_2PdS_2PF_6$*0.15$CH_3NO_2$: C, 35.91, H, 3.40, N, 2.65. Found: C, 36.08, H, 3.58, N, 2.83. ^{1}H-NMR (400MHz, CD_3NO_2): δ = 9.94 (s, 1H), 8.62 (d, J=5.0Hz, 1H), 8.20 (m, 2H), 8.12 (d, J=7.8Hz, 1H), 7.93 (s, 1H), 7.90 (d, J=6.4, 1H), 7.80 (d, J=6.4, 1H), 7.53 (m, 1H), 4.46 (br d, 12Hz), 4.02 (br dd, 12Hz, 12Hz), 3.95-3.45 (br), 3.39 (br d, 16Hz), 3.33-3.15 (br). ^{13}C-NMR (101MHz, CD_3NO_2): δ = 194.04, 164.96, 156.73, 153.48, 153.38, 142.66, 138.49, 136.50, 129.44, 127.11, 126.76, 122.80, 77.28 (br), 77.10 (br), 43.61

(br), 40.82 (br), 39.50 (br), 37.59 (br). ATR-IR (diamond): ν/cm^{-1} = 2929, 2869, 1683, 1603, 1569, 1558, 1487, 1435, 1410, 1314, 1242, 1197, 1128, 1031, 1001, 877, 825, 774, 747, 709, 693, 659, 555. ESI-MS (rel. ab. %): [Pd(ppyCHO)([9]aneS_2O)]$^+$ m/z 452.17 (100%)

Preparation of [Pd(bzq)([9]aneS_2O)](PF_6) (3b) To a solution of [Pd(bzq)(μ-O_2CCH_3)]$_2$ (0.100g, 0.145mmol) in CH_3CN (15mL) was added [9]aneS_2O (0.0478g, 0.291mmol) dissolved in CH_3CN (2mL). The reaction mixture was stirred 18 hr at rt. The solvent removed under reduced pressure, and the residue was redissolved in CH_3OH (20mL). Solid NH_4PF_6 (0.0474g, 0.291mmol) was added and light yellow precipitate formed immediately. After stirring 5 hrs, the solid was collected, rinsed with Et_2O (3x5mL), and dried in vacuo. Yield: 0.159g, 0.274mmol, 94%. Anal. Calc. for $C_{19}H_{20}NPdOS_2PF_6$: C, 38.43, H, 3.39, N, 2.36. Found: C, 38.58, H, 3.36, N, 2.54. ^{1}H-NMR (400MHz, CD_3NO_2): δ = 8.82 (dd, J=5.0, 0.9 Hz, 1H), 8.61 (dd, J=8.2, 0.9 Hz, 1H), 7.92 (d, J=8.0Hz, 1H), 7.83 (d, J=8.0Hz, 2H), 7.73 (dd, J=8.2, 5.0 Hz, 1H), 7.63 (d, J=4.0Hz, 1H), 7.57 (t, J=8.0Hz, 1H), 4.57-4.42 (m, 2H), 4.11-3.97 (m, 2H), 3.92-3.41 (m, 4H), 3.41-3.30 (m, 2H), 3.10-3.29 (m, 2H). ^{13}C-NMR (101MHz, CD_3NO_2): δ = 149.66, 146.11, 136.93, 134.84, 130.33, 127.95, 125.34, 124.81, 123.34 120.83, 119.99, 118.70, 73.30, 71.32, 38.55, 35.97, 33.85, 32.10. ATR-IR (diamond): ν/cm^{-1} = 3326, 2904, 2867, 2360, 1878, 1626, 1607, 1570, 1469, 1453, 1407, 1327, 1293, 1220, 1144, 1130, 1051, 1033, 1026, 1003, 923, 878, 828, 785, 753, 741, 711, 651, 555, 506. ESI-MS (rel. ab. %): [Pd(bzq)([9]aneS_2O)]$^+$ m/z 448.08 (100%)

Preparation of [Pd(btp)([9]aneS_2O)](PF_6) (4b) To a solution of [Pd(btp)(μ-O_2CCH_3)]$_2$ (0.100g, 0.133mmol) in CH_3CN (25mL) was added [9]aneS_2O (0.0437g, 0.266mmol) dissolved

in CH_3CN (2mL). The reaction mixture was bright yellow stirred 22 hr at rt. The solvent removed under reduced pressure and the residue was redissolved in CH_3OH (30mL). Solid NH_4PF_6 (0.0435g, 0.266mmol) was added and a yellow precipitate formed immediately. After stirring 14 hrs, the solid was collected, rinsed with Et_2O (4x5mL), and dried in vacuo. Yield: 0.133g, 0.213mmol, 80%. Anal. Calc. for $C_{19}H_{20}NPdS_3O_2PF_6$ * 0.5 CH_3NO_2: C, 35.68, H, 3.30, N, 3.20. Found: C, 35.60, H, 3.20, N, 3.37. ^{1}H-NMR (400MHz, CD_3NO_2): δ =8.55 (m, 1H), 8.36 (m, 1H), 8.12 (t, J=8.0 Hz, 1H), 7.99 (m, 1H), 7.71 (d, J=8.0Hz, 1H), 7.46 (m, 2H), 7.36 (t, J=6.4Hz, 1H), 4.41 (s broad, 2H), 3.92 (s, broad, 3H), 3.69 (s, broad, 1H), 3.38 (m 6H). ^{13}C-NMR (101MHz, CD_3NO_2): δ = 156.89, 149.40, 147.04, 140.46 137.90, 137.64, 136.05, 122.10, 121.57, 121,51 119.42, 119.19, 116.39, 73.73, 71.70, 41.15, 36.69, 34.59, 30.82. ATR-IR (diamond): ν/cm^{-1} = 3218, 2981, 2911, 2361, 1902, 1604, 1546, 1497, 1470, 1449, 1415, 1379, 1293, 1261, 1236, 1162, 1127, 1063, 1033, 1001, 879, 828, 746, 721, 677, 655, 556, 497, 468. ESI-MS (rel. ab. %): $[Pd(btp)([9]aneS_2O)]^+$ m/z 480.00 (100%)

Preparation of [Pd(pbt)([9]aneS$_2$O)](PF$_6$) (5b) To a solution of $[Pd(pbt)\mu\text{-}O_2CCH_3)]_2$ (0.100g, 0.133mmol) in CH_3CN (23mL) was added [9]aneS$_2$O (0.0437g, 0.266mmol) dissolved in CH_3CN (2mL). The reaction mixture was stirred 16 hr at rt. The solvent removed under reduced pressure, and the residue was redissolved in CH_3OH (20mL). Solid NH_4PF_6 (0.0435g, 0.266mmol) was added, but no significant amount of precipitate formed. Cooling to -10°C facilitate precipitation. The yellow solid was collected and rinsed with Et_2O (3x5mL) and dried in vacuo. Yield: 0.159g, 0.253mmol, 95%. Anal. Calc. for $C_{19}H_{20}NPdO_3S_3PF_6$ * CH_3NO_2: C, 34.97, H, 3.37, N, 4.08. Found: C, 35.16, H, 3.29, N, 4.02. ^{1}H-NMR (400MHz, CD_3NO_2): δ = 8.11 (d, J=8.2, 2H), 7.74 (dd, J=7.1, 1.6Hz 1H), 7.71 (t, J=7.8Hz, 1Hz), 7.59 (m, 2H), 7.35 (m,

2H), 4.40 (s (broad), 2H), 3.91 (td, J=11.6, 3.0 Hz, 2H), 3.67, (s (broad), 2H), 3.60-3.43 (m, 2H), 3.37-3.19 (m, 4H). ^{13}C-NMR (101MHz, CD_3NO_2): δ = 148.40, 145.27, 136.39, 129.72, 127.59, 126.78, 123.91 122.68, 122.41, 121.92, 118.88, 115.10, 73.14-71.68 (2C), 37.45-32.21 (4C). ATR-IR (diamond): ν/cm^{-1} = 3307, 2902, 2863, 2360, 1918, 1551, 1482, 1449, 1415, 1378, 1294, 1273, 1128, 1053, 1033, 1003, 992, 937, 920, 879, 829, 749, 710, 679, 654, 626, 556, 478. ESI-MS (rel. ab. %): [Pd(pbt)([9]aneS_2O)]$^+$ m/z 480.00 (100%)

Syntheses of [Pd(C^N)([9]aneS_3)](PF_6) Complex

Preparation of [Pd(ppyCHO)([9]aneS_3)](PF_6) (2c) To a solution of [Pd(ppyCHO)(μ-O_2CCH_3)]$_2$ (0.0704g, 0.100mmol) in CH_3CN (15mL) was added [9]aneS_3 (0.036g, 0.200mmol). The reaction mixture was stirred 16 hr at rt. The solvent removed under reduced pressure and the residue was redissolved in CH_3OH (10mL). Solid NH_4PF_6 (0.036g, 0.208mmol) was added and a bright yellow precipitate formed immediately. The solid was collected and dried in vacuo. Yield: 0.116g, 0.189mmol, 94%. Anal. Calc. for $C_{18}H_{20}NOPdS_3PF_6$*0.5H_2O: C, 34.71, H, 3.40, N, 2.25. Found: C, 34.57, H, 3.16, N, 2.31. ^{1}H-NMR (400MHz, CD_3NO_2): δ = 9.92 (s, 1H), 8.60 (d, J=5.5Hz, 1H), 8.14 (m, 2H), 7.93 (d, J=7.8Hz, 1H), 7.81 (s, 1H), 7.75 (d, J=7.8, 1H), 7.48 (td, J=6.0, 2.3Hz, 1H), 3.26 (m, 12H, [9]aneS_3). ^{13}C-NMR (101MHz, CD_3NO_2): δ = 188.27, 159.21, 152.64, 147.01, 146.34, 135.80, 132.13, 129.63, 122.47, 120.67, 120.49, 116.87, 27.86 ([9]aneS_3). ATR-IR (diamond): ν/cm^{-1} = 3333, 2982, 2360, 2003, 1682, 1603, 1582, 1482, 1436, 1409, 1379, 1272, 1242, 1187, 1113, 1058, 1030, 1009, 882, 823, 774, 741, 709, 669, 648, 555, 472. ESI-MS (rel. ab. %): [Pd(ppyCHO)([9]aneS_3)]$^+$ m/z 424.08 (100%)

Conflicts of Interest

There are no conflicts of interest to declare.

Acknowledgments

D.E.J acknowledges the Endowed Chair in the Sciences and Carondelet Scholars program, School of Humanities Arts and Sciences, St. Catherine University, the Summer Scholars Undergraduate Research Program, St. Catherine University, and the National Science Foundation: Major Research Instrumentation award #1125975 "MRI Consortium: Acquisition of a Single Crystal X-ray Diffractometer for a Regional PUI Molecular Structure Facility" for funding. D.E.J. also acknowledges Professor Gregory J. Grant, Unviersity of Tennessee at Chattanooga, for generously supplying the ligand [9]aneS_2O. D.A.S.F. gratefully acknowledges the financial support from CNPq, grants 420836/2018-7, 304020/2016-8 and 407682/2013-9, and FAP-DF grants 193.001.596/2017 and 193.001.284/2016. A.A.M. acknowledges financial support by the Coordenação de Aperfeiçoamento de Pessoal de Nível Superior - Brasil (CAPES) - Finance Code 001.

Electronic Supplementary material

CCDC numbers 1895233-1895240 contain the supplementary crystallographic data for this paper. These data can be obtained free of charge from the Cambridge Crystallographic Data Centre via www.ccdc.cam.ac.uk/data_request/cif. Electronic Supplementary Information contains further crystallographic details, NMR spectra, and DFT calculated structure coordinates.

Notes and References

[1] J.J. Topczewski and M.S. Sanford, *Chem. Sci.* 2015, **6**, 70-76.
[2] X. Chen, K.M. Engle, D.-H. Wang and J.-Q. Yu, *Angew. Chem. Int. Ed. Engl.* 2009, **48**, 5094-5115.
[3] X. Wang , D. Leow and J. Q. Yu, *J. Am. Chem. Soc.* 2011, **133**, 13864-13867.
[4] T.W. Lyons, K.L. Hull and M.S. Sanford, *J. Am. Chem. Soc.* 2011, **133**, 4455-4464.
[5] D.C. Powers and T. Ritter, *Nat. Chem.* 2009, **1**, 302-309.
[6] D.C. Powers, D.Y. Xiao, M.A.L. Geibel and T. Ritter, *J. Am. Chem. Soc*. 2010, **132**, 14530-14536.
[7] L.M. Mirica and J.R. Khusnutdinova, *Coord. Chem. Rev.* 2013, **257**, 299-314.
[8] D.E. Janzen, M.A. Bruening, C.A. Sutton and A.R. Sharma, *J. Organomet. Chem.* 2015, **777**, 31-41.
[9] D.E. Janzen, D.G. VanDerveer, L.F. Mehne, D.A. da Silva Filho, J.-L. Bredas and G.J. Grant, *Dalton Trans*. 2008, **9**, 1872-1882.
[10] E. Stephen, A.J. Blake, E. Carter, D. Collison, E.S. Davies, R. Edge, W. Lewis, D.M. Murphy, C. Wilson, R.O. Gould, A.J. Holder, J. McMaster and M. Schröder, *Inorg. Chem.* 2012, **51**, 1450-1461.
[11] E. Stephen, A.J. Blake, E.S. Davies, J. McMaster and M. Schröder, *Chem. Commun.* 2008, 5707-5709.
[12] A.J. Blake, J.A. Greig, A.J. Holder, T.I. Hyde, A. Taylor and M. Schröder, *Angew. Chem. Int. Ed. Engl.* 1990, **29**, 197-198.
[13] J.P. Danks, N.R. Champness, and M. Schröder, *Coord. Chem. Rev.*1998, **174**, 417–468.
[14] C.R. Lucas, W. Liang, D.O. Miller and J.N. Bridson, *Inorg. Chem.*, 1997, **36**, 4508-4513.
[15] G.J. Grant, M.W. Jones, K.D. Loveday, D.G. VanDerveer, W.T. Pennington, C.T. Eagle and L.F. Mehne, *Inorg. Chim. Acta*, 2000, **300**, 250-263.
[16] G.J. Grant, M.E. Botros, J.S. Hassler, D.E. Janzen, C.A. Grapperhaus, M.G. O'Toole and D.G. VanDerveer, *Polyhedron*, 2008, **27**, 3097-3104.
[17] D. Huang, X. Zhang, E.J.L. McInnes, J. McMaster, A.J. Blake, E.S. Davies, J. Wolowska, C. Wilson and M. Schröder, *Inorg. Chem.*, 2008, **47**, 9919-9929.
[18] G.J. Grant, D.F. Galas, M.W. Jones, K.D. Loveday, W.T. Pennington, G.L. Schimek, C.T.Eagle and D.G. VanDerveer, *Inorg. Chem.* 1998, **37**, 5299-5305.
[19] J.P. Tidey, A.E. O'Connor, A. Markevich, E. Bichoutskaia, J. J. P. Cavan, G.A. Lawrance, H. L.S. Wong, J. McMaster, M. Schröder and A.J. Blake, *Cryst. Growth Des.*, 2015, **15**, 115−123.
[20] R. Lindner, B. van den Bosch, M. Lutz, J.N.H. Reek and J.I. van der Vlugt, *Organometallics*, 2011, **30**, 499–510.
[21] E. Peris, *Chem. Rev.* 2018, **118**, 9988–10031.
[22] A.G. Panova, I. Prots, V.S. Fundamensky and K.P. Balashov, *J. Struct. Chem.*, 2010, **51**, 931-934.
[23] S.K. Callear, J. Spencer, H. Patel, J.J. Deadman and M.B. Hursthouse, *J. Chem. Cryst.,* 2011*,* **41**, 523-527.
[24] K.-E. Lee, H.-T. Jeon, S.-Y. Han, J. Ham, Y.-J. Kim and S.W. Lee, *Dalton Trans.* 2009, 0, 6578-6592.

[25] M. Micutz, M. Ilis, T. Staicu, F. Dumitrascu, I. Pasuk, Y. Molard, T. Roisnel and V. Circu, *Dalton Trans*., 2014, **43**, 1151-1161.
[26] A.J. Peloquin, M.B. Smith, G.J. Balaich and S.T. Iacono, *Acta Cryst.* 2017, **E73**, 1279-1281.
[27] V. Novohradsky, J. Yellol, O. Stuchlikova, M.D. Santana, H. Kostrhunova, G. Yellol, J. Kasparkova, D. Bautista, J. Ruiz and V. Brabec, *Chem. Eur. J.*, 2017, **23**, 15294-15299.
[28] L.R. Gahan, *Coord. Chem. Rev.*, 2016, **311**, 168–223.
[29] Giinther, H. NMR Spektroskopie: Grundlagen, Konzepte und Anwendungen der Protonen- und Kohlenstoff-13-Kemresonanz-Spektroskopiei n der Chemie; Georg Thieme Verlag: Stuttgart, New York, 1983; Chapter 9.
[30] H. Nikol, H.-B. Bűrgi, K.I. Hardcastle and H.B. Gray, *Inorg. Chem.*, 1995, **34**, 6319-6322.
[31] T,W. Green, R, Lieberman, N, Mitchell, J.A. Krause-Bauer and W.B. Connick, *Inorg. Chem.*, 2005, **44**, 1955−1965.
[32] A.J. Blake, Y.V. Roberts and M. Schröder, *J. Chem. Soc., Dalton Trans.* 1996, **0**, 1885-1895.
[33] S. Chatterjee, J.A. Krause, W.B. Connick, C. Genre, A. Rodrigue-Witchel and C. Reber, *Inorg. Chem.*, 2010, **49**, 2808-2815.
[34] D.E. Janzen, K. Patel, D.G. VanDerveer and G.J. Grant, *J. Chem.Cryst.*, 2006, **36**, 83-91.
[35] G.J. Grant, K.N. Patel, M.L. Helm, L.F. Mehne, D.W. Klinger and D.G. VanDerveer, *Polyhedron*, 2004, **23**, 1361-1369.
[36] G.J. Grant, N.N. Talbott, M. Bajic, L.F. Mehne, T.J .Holcombe and D.G. VanDerveer, *Polyhedron*, 2012, **31**, 89-97.
[37] CSD evaluation of structures with transition metal pyridine…pyridine intermolecular centroid…centroid distances found most frequent separation around 3.8 Å. C. Janiak, *J. Chem. Soc., Dalton Trans.* 2000, 3885-3896.
[38] J.C.A. Boeyens and S.M. Dobson, Ch.1 Stereochemistry of Metallic Macrocyclics, Ed. I. Bernal in Stereochemistry of Organometallic and Inorganic Compounds, Stereochemical and Stereophysical Behaviour of Macrocycles, vol. 2, Elsevier, Amsterdam, 1987; Chapter 1
[39] R.D. Hancock, S.M. Dobson and J.C.A. Boeyens, *Inorg. Chim. Acta*, 1987, **133**, 221-231.
[40] Recent search of the Cambridge Structural Database v5.40, November 2018 update; The Cambridge Structural Database, C.R. Groom, I.J. Bruno, M.P. Lightfoot and S.C. Ward, *Acta Cryst.*, 2016, **B72**, 171-179.
[41] J.P. Lee, C.L. Keller,A.A. Werlein, D.E. Janzen, D.G. VanDerveer and G.J. Grant, *Organometallics*, 2012, **31**, 6505–6513.
[42] O.K. Kwak, M. Arooj, Y.-J. Yoon, E.D. Jeong and J.K.Park, *Molecules*, 2013, **18**, 12687-12706.
[43] J.K. Park, Y.G. Cho, S.S. Lee and B.G. Kim, *Bull. Korean Chem. Soc.*, 2004, **25**, 85-89
[44] G.J. Grant, C.G. Brandow, D.F. Galas, J.P. Davis, W.T. Pennington, E.J. Valente and J.D. Zubkowski, *Polyhedron*, 2001, **20**, 3333–3342.
[45] J. P. Foster and F. Weinhold, *J. Am. Chem. Soc.*, 1980, **102**, 7211-7218.
[46] A. E. Reed, R. B. Weinstock and F. Weinhold, *J. Chem. Phys.*, 1985, *83*, 735-746.
[47] C.A. Craig and R.J. Watts, *Inorg. Chem.*, 1989, **28**, 309-313.
[48] Gaussian 09, Revision C.01, M.J. Frisch, G.W. Trucks, H.B. Schlegel, G.E. Scuseria, M.A. Robb, J.R. Cheeseman, G. Scalmani, V. Barone, B. Mennucci, G.A. Petersson, H. Nakatsuji, M. Caricato, X. Li, H.P. Hratchian, A.F. Izmaylov, J.Bloino, G.Zheng, J. L. Sonnenberg, M. Hada,

M. Ehara, K. Toyota, R. Fukuda, J. Hasegawa, M. Ishida, T. Nakajima, Y. Honda, O. Kitao, H. Nakai, T. Vreven, J.A. Montgomery, Jr., J.E. Peralta, F. Ogliaro, M. Bearpark, J.J. Heyd, E. Brothers, K.N. Kudin, V.N. Staroverov, T. Keith, R. Kobayashi, J. Normand, K. Raghavachari, A. Rendell, J.C. Burant, S.S. Iyengar, J. Tomasi, M. Cossi, N. Rega, J.M. Millam, M. Klene, J.E. Knox, J.B. Cross, V. Bakken, C. Adamo, J. Jaramillo, R. Gomperts, R.E. Stratmann, O. Yazyev, A.J. Austin, R. Cammi, C. Pomelli, J.W. Ochterski, R.L. Martin, K. Morokuma, V.G. Zakrzewski, G.A. Voth, P. Salvador, J.J. Dannenberg, S. Dapprich, A.D. Daniels, O. Farkas, J.B. Foresman, J.V. Ortiz, J. Cioslowski and D.J. Fox, Gaussian, Inc.,Wallingford CT, 2010.
[49] P. J. Stephens, F.J. Devlin, C.F. Chabalowski and M.J. Frisch, *J. Phys. Chem.*, 1994, **98**, 11623-11627.
[50] A.D. Becke, *J. Chem. Phys.*, 1993, **98**, 5648-5652.
[51] P.J. Hay and W.R. Wadt. *J. Chem. Phys.*, 1985, **82**, 299-310.
[52] M. Cossi, V. Barone, R. Cammi and J. Tomasi, *Chem. Phys. Lett.*, 1996, **255**, 327-335.
[53] C.M. Breneman and K.B. Wiberg, *J. Comp. Chem.*, 1990, **11**, 361-373.
[54] NBO 7.0. E. D. Glendening, J. K. Badenhoop, A. E. Reed, J. E. Carpenter, J. A. Bohmann, C. M. Morales, P. Karafiloglou, C. R. Landis, and F. Weinhold, Theoretical Chemistry Institute, University of Wisconsin, Madison, WI (2018)
[55] C. Peng and H.B. Schlegel, *Isr. J. Chem.*, 1993, **33**, 449-454.
[56] X. Li and M.J. Frisch, *J. Chem. Theory Comput.*, 2006, **2**, 835-839.
[57] T. Lu and F. Chen, *J. Comput. Chem.*, 2012, **33**, 580-592.
[58] Oxford Cryosystems Ltd, Oxford.
[59] Rigaku Americas and Rigaku (2011) CrystalClear. Rigaku Americas and Rigaku Corporation, The Woodlands, TX.
[60] R. Jacobson, REQAB (1998) Molecular Structure Corporation, The Woodlands, Texas, USA.
[61] G.M. Sheldrick, *Acta Cryst*., 2008, **A64**, 112–122.
[62] Rigaku (2014). CrystalStructure. Version 4.1. Rigaku Corporation, Tokyo, Japan.

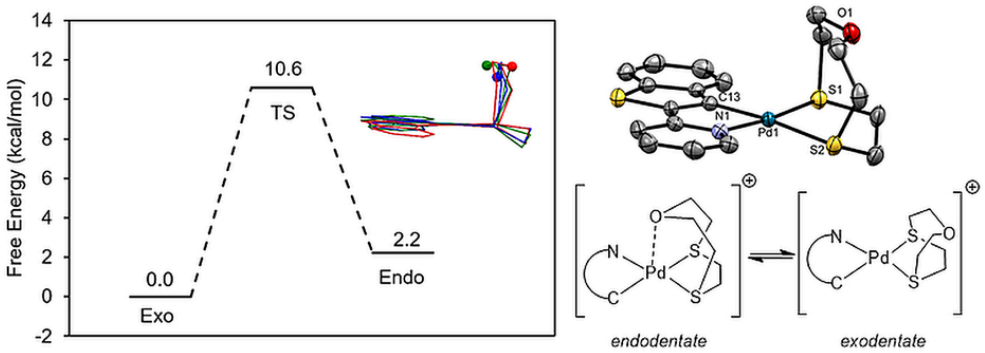

80x28mm (300 x 300 DPI)